frontiers in Earth Science

ORIGINAL RESEARCH
published: 28 October 2021
doi: 10.3389/feart.2021.716416

Anthropogenic Inputs of Terrestrial Organic Matter Influence Carbon Loading and Methanogenesis in Coastal Baltic Sea Sediments

Tom Jilbert[1,2,3], Greg Cowie[4], Luukas Lintumäki[3], Sami Jokinen[1,5], Eero Asmala[1,2], Xiaole Sun[6], Carl-Magnus Mörth[6], Alf Norkko[2,6] and Christoph Humborg[2,6]*

[1]Aquatic Biogeochemistry Research Unit, Ecosystems and Environment Research Program, Faculty of Biological and Environmental Sciences, University of Helsinki, Helsinki, Finland, [2]Tvärminne Zoological Station, University of Helsinki, Hanko, Finland, [3]Department of Geosciences and Geography, Faculty of Science, University of Helsinki, Helsinki, Finland, [4]Marine Geosciences Group, School of Geosciences, Edinburgh University, Edinburgh, United Kingdom, [5]Marine Geology, Geological Survey of Finland (GTK), Espoo, Finland, [6]Baltic Sea Centre, Stockholm University, Stockholm, Sweden

OPEN ACCESS

Edited by:
Christian März,
University of Leeds, United Kingdom

Reviewed by:
Tobias Goldhammer,
Leibniz-Institute of Freshwater Ecology and Inland Fisheries (IGB), Germany
Laura Lapham,
University of Maryland Center for Environmental Science (UMCES), United States

***Correspondence:**
Tom Jilbert
tom.jilbert@helsinki.fi

Specialty section:
This article was submitted to Biogeoscience, a section of the journal Frontiers in Earth Science

Received: 28 May 2021
Accepted: 08 October 2021
Published: 28 October 2021

Citation:
Jilbert T, Cowie G, Lintumäki L, Jokinen S, Asmala E, Sun X, Mörth C-M, Norkko A and Humborg C (2021) Anthropogenic Inputs of Terrestrial Organic Matter Influence Carbon Loading and Methanogenesis in Coastal Baltic Sea Sediments. Front. Earth Sci. 9:716416. doi: 10.3389/feart.2021.716416

Coastal regions globally have experienced widespread anthropogenic eutrophication in recent decades. Loading of autochthonous carbon to coastal sediments enhances the demand for electron acceptors for microbial remineralization, often leading to rearrangement of the sediment diagenetic zonation and potentially enhancing fluxes of methane and hydrogen sulfide from the seafloor. However, the role of anthropogenic inputs of terrestrial organic matter ($OM_{terr.}$) in modulating diagenesis in coastal sediments is often overlooked, despite being of potential importance in regions of land-use and industrial change. Here we present a dated 4-m sediment and porewater geochemistry record from a eutrophic coastal location in the northern Baltic Sea, to investigate sources of recent carbon loading and their impact on modern diagenetic processes. Based on an end-member mixing model of sediment N/C ratios, we observe that a significant fraction of the late-20th century carbon loading at this location was contributed by $OM_{terr.}$. Furthermore, analysis of lignin in this material shows depleted ratios of syringyl/vanillyl (S/V) and cinnamyl/vanillyl (C/V) phenols, indicative of enhanced inputs of woody gymnosperm tissue likely from forest industries. The rapid loading of organic matter from combined terrestrial and autochthonous sources during the late 20th century has stimulated methanogenesis in the sediment column, and shoaled the sulfate-methane transition zone (SMTZ) to a depth of 5–20 cm. Optical parameters of colored dissolved organic matter confirm that $OM_{terr.}$ is actively degrading in the methanogenic layer, implying a role for this material in diagenetic processes. Porewater CH_4, SO_4^{2-} δ^{13}C-DIC, and $\sum S^{2-}$ data suggest that the modern SMTZ is a broad zone in which organoclastic sulfate reduction, methanogenesis and anaerobic oxidation of methane (AOM) co-occur. However, fluxes of CH_4 and SO_4^{2-} show that rates of these processes are similar to other marine locations with a comparably shallow SMTZ. We suggest that the shallow depth of the modern SMTZ is the principal reason for high observed diffusive and ebullitive methane fluxes from sediments in this area. Our results highlight that anthropogenic activities lead to multiple pathways of carbon loading to coastal

sediments, and that forest industry impacts on sedimentation in the northern Baltic Sea may be more widespread than previously acknowledged.

Keywords: terrestrial organic matter, forestry, lignin, diagenesis, methane, blue carbon, baltic sea

INTRODUCTION

Anthropogenic impacts on coastal environments have accelerated in parallel with industrialization during the late 20th century (Diaz and Rosenberg, 2008). Among the most widespread and important impacts is eutrophication, defined as an increased supply of organic matter to a coastal ecosystem (Nixon, 1995), and often primarily driven by enhancement of autochthonous productivity due to loading of nutrients such as nitrogen and phosphorus (Bonsdorff et al., 1997; Anderson et al., 2002). Eutrophication increases the amount of fixed organic carbon in coastal ecosystems and alters the primary producer community structure (Heisler et al., 2008), consequently raising the oxygen demand of microbial remineralization of organic matter (OM) (Middelburg and Levin, 2009; Breitburg et al., 2018). In turn, consumption of oxygen leads to further ecosystem impacts associated with benthic hypoxia (Carstensen et al., 2014; Rabalais et al., 2014). Because a significant fraction of OM remineralization in shallow coastal systems takes place in the underlying sediments, eutrophication can severely impact rates of microbial processes in the sediment column. Ultimately, these processes dictate the rate of organic carbon turnover and burial (Arndt et al., 2013) and hence play a critical role in the global carbon cycle.

One of the key consequences of eutrophication for coastal sediment microbial processes is to enhance rates of anaerobic remineralization after the exhaustion of oxygen (Middelburg and Levin, 2009). Organoclastic sulfate reduction is the dominant pathway of anaerobic remineralization in marine sediments (Jorgensen, 1982; Canfield, 1991; Bowles et al., 2014), but in settings with low salinity and high flux of sedimenting OM, sulfate may become completely exhausted within the upper sediment column (e.g., Slomp et al., 2013; Thang et al., 2013). In such cases, a significant fraction of OM remineralization occurs through methanogenesis (Rooze et al., 2016), creating the potential for emissions of this potent greenhouse gas to the water column and ultimately the atmosphere (Bange et al., 1994; Gelesh et al., 2016; Humborg et al., 2019; Myllykangas et al., 2020a). Many studies have demonstrated the presence of methane within the uppermost meter of the sediment column in low-salinity coastal settings (e.g., Albert et al., 1998; Martens et al., 1998; Mogollon et al., 2011; Egger et al., 2015), and human-impacted estuaries are considered hotspots for methane emissions (Borges and Abril, 2011). Because such emissions may offset the climate benefits of carbon burial (Dean et al., 2018), it is essential to understand the controls on methanogenesis in human-impacted coastal sediments.

Associated to changes in vertical zonation of primary anaerobic remineralization pathways, eutrophication can also strongly modify the network of secondary microbial processes in the sediment column. For example, a key consequence of enhanced methanogenesis in human-impacted systems is enhanced rates of anaerobic oxidation of methane (AOM). This process proceeds mainly through coupling to sulfate reduction at the so-called sulfate methane transition zone (SMTZ) (Knittel and Boetius, 2009), but can also be coupled to reduction of nitrate (Ettwig et al., 2010) or metal oxides (Beal et al., 2009; Sivan et al., 2011; Egger et al., 2015). Crucially, AOM strongly reduces the fluxes of methane from the sediments to the water column relative to the amount of methane produced during sedimentary methanogenesis, thus acting as a filter for methane emissions (Dean et al., 2018).

In addition to inputs of autochthonous OM, coastal sediments also receive carbon loading from terrestrial organic matter ($OM_{terr.}$) (Blair and Aller, 2012). Up to 200 Tg particulate organic carbon (POC) are delivered by rivers to coastal environments annually (Schlunz and Schneider, 2000), while a similar flux has been calculated for dissolved organic carbon (DOC) (Dai et al., 2012). The DOC contribution typically dominates $OM_{terr.}$ inputs in boreal systems (e.g. Mattsson et al., 2005). The importance of DOC inputs for coastal sediment carbon loading in the Baltic Sea is not well constrained, but several studies have suggested that salt-mediated flocculation may transfer carbon from the dissolved to particulate phase at the land-sea transition (Sholkovitz et al., 1978; Asmala et al., 2014; Jilbert et al., 2018). Typically, the reactivity of $OM_{terr.}$ in microbial remineralization is considered lower than that of autochthonous material (Hedges et al., 2000). This is due to a combination of its refractory molecular composition, being dominated by lignin, cellulose and cutin (de Leeuw and Largeau, 1993) and physical association to protective minerogenic material prior to deposition (Mayer, 1994; Hedges and Keil, 1995). However, riverine fluxes, molecular composition and biological reactivity of OM_{terr} have been shown to be sensitive to anthropogenic activities such as deforestation, ditching, agriculture and industry (e.g., Lambert et al., 2017; Asmala et al., 2019; Deininger and Frigstad, 2019; Landsman-Gerjoi et al., 2020). Rapid inputs of such "anthropogenic" $OM_{terr.}$ to coastal sediments may be expected to confer higher reactivity to $OM_{terr.}$ in the sediment column. Yet, few studies have explicitly investigated the impacts of anthropogenic $OM_{terr.}$ inputs on coastal sediment biogeochemistry.

In boreal regions, a key driver of anthropogenic $OM_{terr.}$ inputs to the marine environment over the last century is forestry and the associated paper and pulp industry. Forest industry processes, including debarking, pulping, bleaching and washing (Ali and Sreekrishnan, 2001), have introduced large point-source emissions of raw and processed $OM_{terr.}$ to aquatic systems, in many cases proximal to the coastal environment (Pocklington and McGregor, 1973; Louchouarn et al., 1999; Brandenberger et al., 2011). The molecular composition of solid forest industry

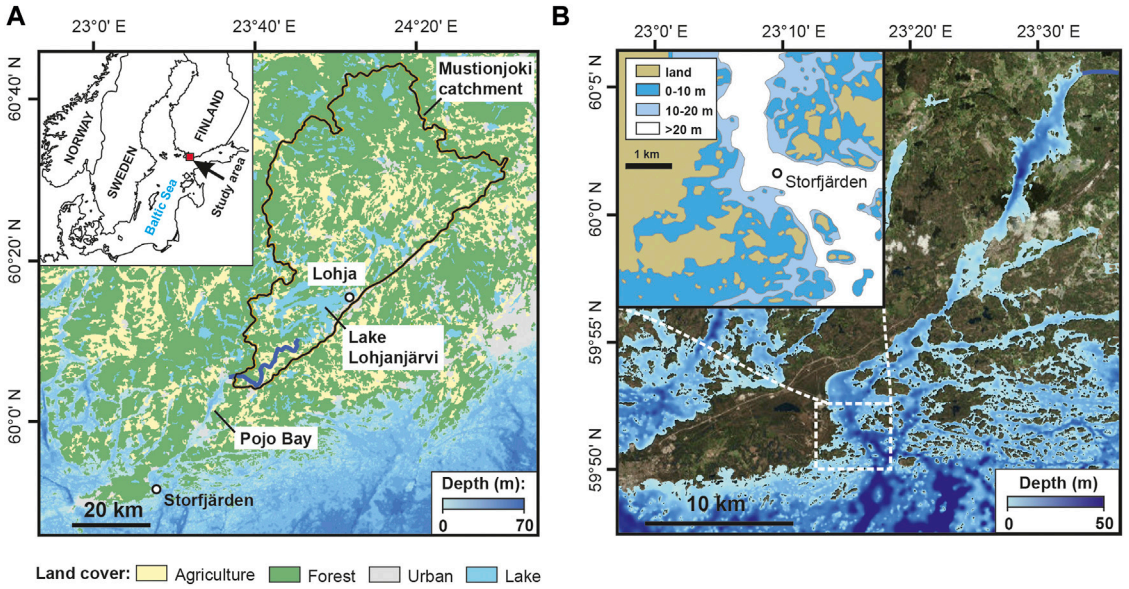

FIGURE 1 | Location of the study. **(A)** (inset) Study area in the northern Baltic Sea. (main) Catchment of the Mustionjoki river (black) showing the location of the city of Lohja and adjacent Lake Lohjanjärvi. Blue line shows the Mustionjoki river itself, connecting the catchment to the Pojo Bay estuarine system draining into Storfjärden. **(B)** (main) location of Storfjärden at the southern end of the estuary. (inset) zoom of the coring location in Storfjärden.

wastes in sediments includes the major wood polymers cellulose and lignin (Louchouarn et al., 1997; Dahlberg et al., 2020), together with a wide array of additional compounds from the raw material and its treatment processes, including tannins, resin acids, and polychlorinated biphenyls (PCBs) (Lacorte et al., 2003). Sedimentary contents of such materials have been shown to vary with distance from industrial sources, with the most concentrated deposits (e.g., cellulose-rich *fiberbanks*) consisting of nearly pure organic material (Dahlberg et al., 2020; Dahlberg et al., 2021).

To date, several studies have used organic biomarkers such as lignin phenols and persistent organic pollutants (POPs) to identify the presence of forest industry-derived anthropogenic $OM_{terr.}$ in boreal coastal sediments, and to quantify its local contribution to total $OM_{terr.}$ or total sedimentary organic matter (e.g., Louchouaran et al., 1997; 1999; Dahlberg et al., 2020). However, few studies have combined these analyses with a porewater biogeochemistry approach to determine the potential role of such inputs on sediment diagenetic processes, including methanogenesis. This is an important gap in knowledge, since $OM_{terr.}$ has been shown to promote methanogenesis in lakes (Tittel el al., 2019) and fiberbank material in particular shows strong methanogenic potential (Kokko et al., 2018). Here, we employ a comprehensive analysis of sediment bulk inorganic and organic chemical parameters, including lignin phenol analysis, coupled to detailed porewater chemical profiling, to determine the impacts of recent anthropogenic $OM_{terr.}$ inputs on diagenesis at a site in the northern Baltic Sea. The site is located tens of kilometers from the nearest forest industry point source, allowing investigation of larger spatial-scale impacts of anthropogenic $OM_{terr.}$ than previous studies focused on fiberbanks close to industrial point sources.

SITE DESCRIPTION

The Baltic Sea is a landlocked brackish marine system in northern Europe with a N-S salinity gradient of 3–15 (Leppäranta and Myrberg, 2009). The whole Baltic Sea was strongly eutrophied by nutrient loading during the 20th century (Gustafsson et al., 2012), leading to the development of widespread deep water hypoxia and anoxia in the central basins (Conley et al., 2009). Many coastal areas have shown localized trends towards oxygen depletion during recent decades, as a consequence of direct nutrient inputs from adjacent land areas leading to coastal eutrophication (Conley et al., 2011). The contribution of $OM_{terr.}$ to Baltic Sea sediments as a whole is estimated as ≤30% of total OM, with a N-S compositional gradient from gymnosperm-to angiosperm-dominated material (Miltner and Emeis, 2001). A recent study demonstrated clearly higher $OM_{terr.}$ contributions to sedimentary carbon in northern areas such as the Gulf of Bothnia and Gulf of Finland (Nilsson et al., 2021).

This study focuses on the Storfjärden site on the Finnish coast of the Gulf of Finland in the northern Baltic Sea (**Figure 1**). Storfjärden is a shallow coastal basin forming part of the Tvärminne archipelago system at the mouth of the Pojo Bay estuary, draining the Mustionjoki river catchment in southern Finland. Since the most recent deglaciation at 12250 cal year BP, Storfjärden has been successively covered by late- and post-glacial lacustrine clays and most recently by brackish-water muds (Virtasalo et al., 2014; Virtasalo., 2019). The Gulf of Finland

TABLE 1 | Sediment cores on which geochemical analyses of porewaters and sediments were performed, along with depth intervals presented in this study. For GEMAX cores from 2015, sediment parameters derive from the April core, while porewater parameters derive from the June core.

	Porewater parameters							Sediment parameters			
	NH_4^+	Alk	δ^{13}C-DIC	S (ICP-OES)	$\sum S^{2-}$	CH_4	DOM (peak C, HIX)	Pb_{tot}, $^{206/207}Pb$	C, N	Lignin phenols	Fe, Mn, S (ICP-OES)
GEMAX April/June 2015 0–40 cm	●				●[a]			●	●	●	●[a]
GEMAX Sept. 2018 0–60 cm		●	●	●		●					
GEMAX June 2020 0–60 cm							●				
Piston Sept. 2017 40–400 cm	●							●	●	●	●
Piston Sept. 2018 60–550 cm		●	●	●		●	●				

[a]*Data reproduced from Jilbert et al. (2018).*

coastal areas were affected by eutrophication during the 20th century (Weckström, 2006), and the majority of the OM in the modern sediments is derived from autochthonous production (Jilbert et al., 2018). However, Jokinen et al. (2020) measured elevated contents of $OM_{terr.}$ in nearby sediments during the depositional interval corresponding to the late 20th century, suggesting an anthropogenic influence on $OM_{terr.}$ fluxes from the Mustionjoki catchment during this period. The city of Lohja in the southern part of the catchment has been a major center of the Finnish pulp and paper industry since the early 20th century (Katko et al., 2005).

MATERIALS AND METHODS

Sediment Coring

Sediments were collected from the Storfjärden site (33 m water depth, **Figure 1**) during various sampling campaigns from 2015 to 2020, onboard the vessels R/V Saduria, R/V Electra and R/V Augusta (**Table 1**). A twin-barrel GEMAX coring device was used to recover the intact sediment surface and approximately the uppermost half meter of the sediment column. A piston corer onboard R/V Electra was used to recover longer sediment cores (max. length 4.5 m in September 2017; 5.5 m in September 2018). Seasonal changes in sediment and porewater chemistry on the decimeter scale are known to be minimal at this site (Myllykangas et al., 2020a), hence the figures in this paper present combined data from multiple sampling campaigns.

Porewater Sampling and Treatment

Porewater samples for most parameters were collected with Rhizons™ (pore size 0.15 µm). For each core, a vertical series of holes (diameter 4 mm) was pre-drilled into the liner and taped prior to sampling (resolution 2 cm for GEMAX cores, 10 cm for piston cores). After core recovery, the tape was penetrated and Rhizons™ inserted. Porewater was collected under vacuum in an attached plastic syringe and transferred to vials for subsampling. After transfer from the syringes, subsampling and treatment were performed immediately to minimize oxidation artefacts. Subsamples for analysis of dissolved sulfur (S) by ICP-OES were acidified with 10–20 µl 65% HNO_3 per ml. Subsamples for analysis of ammonium were frozen. Subsamples for analysis of δ^{13}C-DIC were injected into helium-flushed glass vials (Labco 12 ml Exetainer, model 738W) pre-loaded with 0.1 ml H_3PO_4 per ml. Finally, subsamples for analysis of total alkalinity (Alk_T), and of optical characteristics of colored and fluorescent dissolved organic matter (CDOM and FDOM), were stored at 4°C. For determination of total dissolved sulfide ($\sum S^{2-}$) in the GEMAX core of June 2015, a series of syringes were pre-loaded with 1 ml 10% w/v zinc acetate solution prior to sampling with Rhizons™. Samples were stored at room temperature after precipitation of zinc sulfide (ZnS).

Porewater samples for dissolved methane were collected as described in Egger et al. (2015) and Myllykangas et al. (2020a). Briefly, core liners were pre-drilled with a series of holes (diameter 30 mm) and taped prior to sampling (resolution 2.5 cm for GEMAX cores, 10 cm for piston cores). A 10 ml sample of wet sediment was extracted using a cut-off plastic syringe and transferred directly into a 65-ml glass bottle containing supersaturated NaCl solution. The bottles were closed with a butyl rubber stopper and screw cap. A headspace of 10 ml N_2 gas (purity 5.0) was injected through the stopper within 24 h of sampling and bottles were stored inverted until analysis.

Porewater Analyses

Dissolved S was determined by ICP-OES after dilution (Thermo iCAP 6000 at University of Helsinki), and is assumed to predominantly represent SO_4^{2-}. Hydrogen sulfide (H_2S) is lost during acidification hence does not contribute to dissolved S in the ICP-OES subsample (Jilbert and Slomp, 2013). We acknowledge that at low SO_4^{2-} concentrations, such as in deeper layers of the sediments, non-zero dissolved S values may indicate the presence of dissolved organic sulfur (Jilbert et al., 2020). However, the present study focuses on S gradients in the near-surface sediments, where this fraction is considered negligible, hence we assume dissolved S ≈ SO_4^{2-}. Reproducibility of the ICP-OES analyses is <5% RSD. Dissolved ammonium (NH_4^+) was determined by the indophenol method (Koroleff, 1976) using an autoanalyzer (Lachat QuikChem 8000, reproducibility <5% RSD). Analysis of δ^{13}C-DIC in headspace gas from the H_3PO_4-acidified vials was performed on a Thermo Gasbench II coupled to a MAT 253 mass spectrometer at Stockholm University and is reported in conventional delta notation relative to Vienna PeeDee Belemnite (VPDB). Standard deviation was less than 0.1‰.

Total alkalinity (Alk_T) was determined by HCl titration with a Metrohm Titrando 809 (reproducibility <2% RSD).

Total dissolved sulfide ($\sum S^{2-}$) concentrations in the Zn acetate-treated samples from June 2015 were determined by spectrophotometry (670 nm) after direct addition of an acidic solution of $FeCl_3$ and n,n-dimethyl-p-phenylenediamine (Cline, 1969; Reese et al., 2011) to the sample vials. The procedure dissolves the ZnS precipitate and immediately complexes S as methylene blue for spectrophotometric analysis. Total dissolved sulfide concentrations were calibrated against a series of standard solutions of $Na_2S{\cdot}3H_2O$, fixed in Zn acetate in the same manner as the samples. The exact concentration of S in the $Na_2S{\cdot}3H_2O$ stock solution was determined by iodometric titration (Burton et al., 2008).

Dissolved methane (CH_4) concentrations were determined by gas chromatography. Subsamples of 1 ml were taken from the headspace of each 65 ml glass bottle with a gas-tight glass syringe and transferred to evacuated 12-ml glass tubes with a butyl rubber septum (LabCo Exetainer™ model 839W). Exetainers were then pressurized with 20 ml N_2 (purity 5.0). The mole fraction of methane in headspace of the samples was analyzed with a FID-equipped gas chromatograph (Agilent Technologies 7890B, University of Helsinki) against a standard series of known CH_4 concentrations. Porewater concentrations were calculated assuming quantitative evolution of methane into the headspace from the original 10 ml wet sediment sample, using the measured porosity profile from sediment sample processing. Due to use of unpressurized coring apparatus and sampling on deck, partial degassing of CH_4 from the cores after recovery cannot be avoided (e.g. Thang et al., 2013; Egger et al., 2016). The saturation concentration range of CH_4 at *in situ* salinity, 1 atm pressure and range of temperatures experienced on deck is therefore given in the plots of dissolved CH_4 concentrations to assess the potential impact of degassing.

Absorbance of CDOM was determined using a Shimadzu 2401PC spectrophotometer with 5-cm quartz cuvette (spectral range from 200 to 800 nm with 1 nm resolution). Excitation–emission matrices (EEMs) of FDOM were determined with a Varian Cary Eclipse spectrofluorometer (Agilent). Ultrapure water was used as the blank for all samples, and EEMs were corrected and optical proxies extracted as in Asmala et al. (2018).

Porewater Data Processing

GEMAX and piston core profiles were spliced on the basis of overlaps in the NH_4^+ and Alk_T data. For the purposes of this study, we apply the simplification outlined in Miller et al. (2017) to utilize the Alk_T data directly to investigate gradients in dissolved inorganic carbon (DIC) as represented by the bicarbonate ion HCO_3^-:

$$A1K_T \approx [HCO_3^-] + [HS^-] \quad (1)$$

In practice, our maximum detected value of HS^- (determined from $\sum S^{2-}$ analyses) contributed less than 2% of the Alk_T value at the equivalent depth, which is similar to the precision of the titration method. Therefore, we assume $Alk_T \approx [HCO_3\text{-}] \approx [DIC]$.

Values of $\Delta[DIC]$ and $\Delta[SO_4^{2-}]$, i.e. *change* in concentration between water column and a given depth in the sediments, are often used to investigate diagenetic process at the SMTZ (e.g. Chatterjee et al., 2011). We estimated these values relative to typical local bottom water [DIC] and $[SO_4^{2-}]$ of 2.0 mmol/L and 6.0 mmol/L, respectively. Gradients of [DIC], $[CH_4]$ and $[SO_4^{2-}]$ in the vicinity of the SMTZ (all sampled during the September 2018 campaign) were estimated from linear regression lines through a subset of data points from the profiles of each parameter. Fick's First Law was applied to calculate diffusive fluxes of each species, using the measured porosity profile and assuming a constant temperature of 7.5°C (determined from bottom water during sampling):

$$J = \frac{D \cdot \varphi}{\theta^2} \frac{dC}{dz} \quad (2a)$$

$$\theta^2 = 1 - ln(\varphi)^2 \quad (2b)$$

in which J = flux (initially calculated in $\mu mol\ cm^{-2}\ s^{-1}$; here negative values indicate downwards fluxes towards the SMTZ, and vice versa), D = ion-specific diffusion coefficient, corrected for temperature, taken from Boudreau (1997), φ = porosity and θ =tortuosity, defined as per Boudreau (1997), and $\frac{dC}{dz}$ is the concentration gradient as given by the linear regression line.

Although fluctuation in temperature in the core profile is expected with depth in the sediments due to propagation of seasonal changes in bottom water temperature (e.g., Mogollon et al., 2011; Mueller et al., 2016), the potential error in calculated fluxes is expected to be <20% for absolute values of each species (based on the climatological range of bottom water temperature at the site (Merkouriadi and Leppäranta, 2015) and <3% for the flux ratios, due to the parallel effects of temperature on all species.

For assessing the optical fingerprint of porewater DOM, the magnitude of the C-fluorescence peak (Coble, 1996) and humification index (HIX; Zsolnay et al., 1999) were calculated from the measured and corrected EEMs. Absorbance spectra and EEMs were processed using the cdom and eemR packages for R software (Massicotte and Markager 2016; Massicotte 2019, respectively).

Sediment Sampling, Processing and Analysis

Sediment cores were sliced on deck (GEMAX) or in the laboratory (piston) at intervals of 1 cm (uppermost 10 cm) or 2 cm (>10 cm depth) into plastic bags. Samples were stored frozen until further processing, then freeze-dried and homogenized in an agate mortar. Volumetric porosity was estimated from weight loss on freeze drying, assuming a sediment density of $2.5\ g\ cm^{-3}$. Dried subsamples were analyzed for total carbon and nitrogen contents by thermal combustion elemental analysis (LECO TruSpec Micro, University of Helsinki, analytical precision and accuracy <10% RSD). A subsample of 3–4 mg dried sediment was weighed into tin cups and loaded into an autosampler rosette. Inorganic carbon and nitrogen forms are considered negligible in this setting, hence measured total carbon and nitrogen concentrations are

TABLE 2 | Lignin phenol oxidation products analyzed in this study. Codes indicate provenance as described by Hedges and Ertel (1982). G = gymnosperms, woody tissue; g = gymnosperms, non-woody tissue; A = angiosperms, woody tissue; a = angiosperms, non-woody tissue.

Vanillyl phenols (V)		Syringyl phenols (S)		Cinnamyl phenols (C)	
GgAa	Vanillin	Aa	Syringaldehyde	ga	Coumaric acid
GgAa	Acetovanillone	Aa	Acetosyringone	ga	Ferulic acid
GgAa	Vanillic acid	Aa	Syringic acid		

considered equivalent to the concentrations of the organic forms (C_{org}, N_{org}).

Dried subsamples were prepared for further bulk elemental analysis by a triple-acid digestion procedure. From 0.1–0.2 g of sediment was extracted over night with 5 ml HF (45%) and 5 ml of mixed $HClO_4$ (70%)/HNO_3 (65%) (volumetric ratio 3:2) at 90°C in closed teflon vials. The acids were then evaporated at 160°C until samples displayed a gel-like consistency, and 15 ml 1 M HNO_3 was added to re-dissolve the material. Where necessary, further dilution was applied prior to analysis. Extracts were analyzed by ICP-OES (Thermo iCAP 6000, Helsinki, analytical precision <5% RSD) for total iron (Fe_{tot}), managanese (Mn_{tot}) and sulfur (S_{tot}), and by ICP-MS (Thermo Element 2, Utrecht University) for total lead (Pb_{tot}) and stable isotopic ratios of Pb ($^{206}Pb/^{207}Pb$, analytical precision <5% RSD). Reproducibility of the total extraction procedure determined by replicates was <15% RSD. Absolute accuracy of the entire sample preparation, digestion, and analysis, as determined by comparison with standard reference material ISE-921 (Van der Veer, 2006), was <15% for Fe, Mn and S and <25% for Pb.

Dried subsamples from selected depths were subjected to alkaline CuO oxidation in closed vessels in a furnace for the extraction of lignin phenols (slight modification to Hedges and Ertel, 1982). Briefly, 0.5 g sediment was added to the vessel with 1 g purified CuO and 100 mg $Fe(NH_4)_2(SO_4)_2{\cdot}6H_2O$ (to scavenge O_2), 7.0 ml of 8% (wt/wt) aqueous NaOH, and a small stainless steel bar agitator. The oxidation procedure was carried out for 3 h at 155°C, after which the mixture was acidified to pH 1 with HCl. Organic oxidation products were then extracted with purified ethyl acetate and then concentrated, first by rotoevaporation and then to near dryness with a flow of N_2 over the final ~1-ml volume, in the presence of anhydrous $NaSO_4$ to remove moisture. The concentrated extract was re-dissolved in pyridine with trans-cinnamic acid as internal standard and N,O-bis(trimethylsilyl) trifluoroacetamide (BSTFA) as derivitizing agent. Samples were analyzed for concentrations of 8 vanillyl, syringyl and cinnamyl lignin phenols (**Table 2**) by GC-MS at the University of Edinburgh.

Sediment Data Processing

A simple two end-member mixing model was used to investigate bulk OM sources. The calculation uses only the molar N/C ratio of organic matter, and end-member values, N/C_{EM}, based on the studies of Goñi et al. (2003) and Jilbert et al. (2018):

$$\%\,OC_{phyt} = \frac{\left(N/C_{sample} - N/C_{EM-terr}\right)}{\left(N/C_{EM-phyt} - N/C_{EM-terr}\right)} \times 100 \quad (3)$$

$$\%\,OC_{terr} = 100 - \%\,OC_{phyt} \quad (4)$$

where $\%OC_{phyt.}$ and $\%OC_{terr.}$ are the respective contributions of phytoplankton and terrestrial material to total sedimentary organic carbon (OC), with $N/C_{EM\text{-}terr} = 0.04$, and $N/C_{EM\text{-}phyt} = 0.13$. The mixing model assumes that terrestrial plant matter and phytoplankton are the only sources of organic material, that their N/C values are spatially and temporally fixed at the end-member values, and that these values do not alter significantly during sedimentation and burial of organic matter.

Absolute and relative concentrations of lignin phenol oxidation products were computed according to standard notations. These include: $\sum_8$ = sum of 8 measured phenols reported as $\mu g\,g^{-1}$ sediment; Λ_8 = sum of 8 phenols reported as mg/100g C; Λ_V = sum of 3 vannilyl phenols reported as mg/100g C (Bianchi and Canuel, 2011). Phenol compositions are expressed through ratios of the summed cinnamyl and syringyl phenols to the summed vannilyl phenols (C/V and S/V, respectively) (**Table 2**).

Age vs Depth Model

An age vs depth model for the Storfjärden site was produced from the sediment Pb_{tot} data, combining samples from the GEMAX core of June 2015 with the piston core of September 2017 (**Figure 2**). We used seven tie-points in the combined Pb_{tot} profile, identified as per Brännvall et al. (1999), Zillen et al. (2012) and Jokinen et al. (2018), and assumed to represent known temporal changes in the deposition of anthropogenic Pb over the last two millennia. Age uncertainty of pre-20th century tie-points was set at 25 years, while that of the 1970 tie-point was set at 10 years. Depth uncertainties were set at 4–8 cm. The model was produced from the tie-points using the *Undatable* software of Lougheed and Obrochta (2019), applying 10^5 simulations with an xfactor of 0.1 and 15% bootstrapping. Of these, the xfactor dictates the maximum allowable variation in sediment accumulation rate between all pairs of age-depth constraints, while the bootstrapping percentage determines the number of tie-points that are randomly excluded from the simulations. The approach takes into account uncertainty in both age and depth, with uncertainty allowed to increase with distance from tie-points, and uses a Bayesian approach to estimate a probability-density cloud for the upper 310 cm of the sediment. A subset of tie-points in the Pb_{tot} profile were checked by comparison with $^{206}Pb/^{207}Pb$ data, but the latter were not used in the construction of the model due to the observed low signal-to-noise ratio in the profile. Linear sedimentation rate (LSR) and mass accumulation rate (MAR) were estimated for each segment between tie-points using the measured porosity profile. Accumulation rate of $OC_{terr.}$ was estimated for each sampled interval from the estimated content of OC_{terr} (**Eq. 4**) and MAR of the corresponding segment.

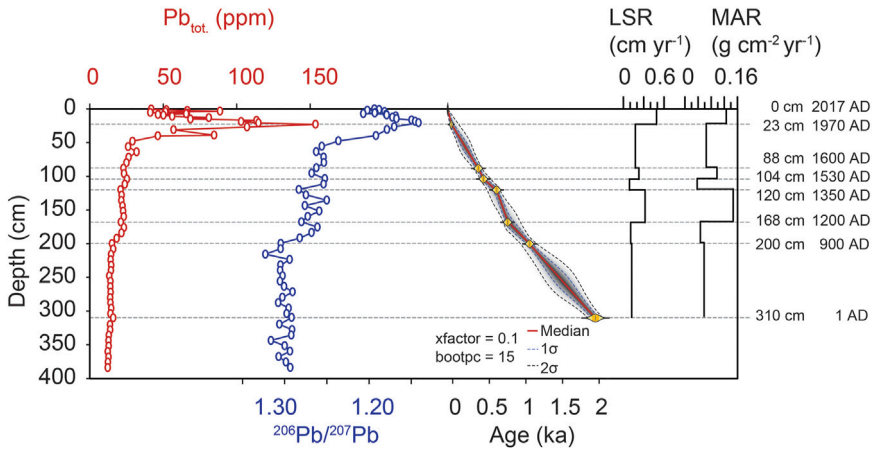

FIGURE 2 | Construction of the age vs depth model for the Storfjärden site. Note that Age 0 ka = AD 1950. The figure combines data from the GEMAX core of April 2015 (0–40 cm) and the piston core of September 2017 (40–400 cm). Seven tie-points in the Pb_{tot} profile (red), in addition to the sediment-water interface, were used to constrain the chronology based on temporal changes in anthropogenic Pb deposition (Brännvall et al., 1999; Jokinen et al., 2018). The *Undatable* software generates a probability-density cloud (grey shaded region, note 1σ and 2σ windows) between the tie-points. Age and depth uncertainty of the tie-points themselves is indicated by the yellow symbols. The $^{206}Pb/^{207}Pb$ profile is shown for comparison. Note that these data were not used to constrain tie-points due to observed low signal-to-noise ratio.

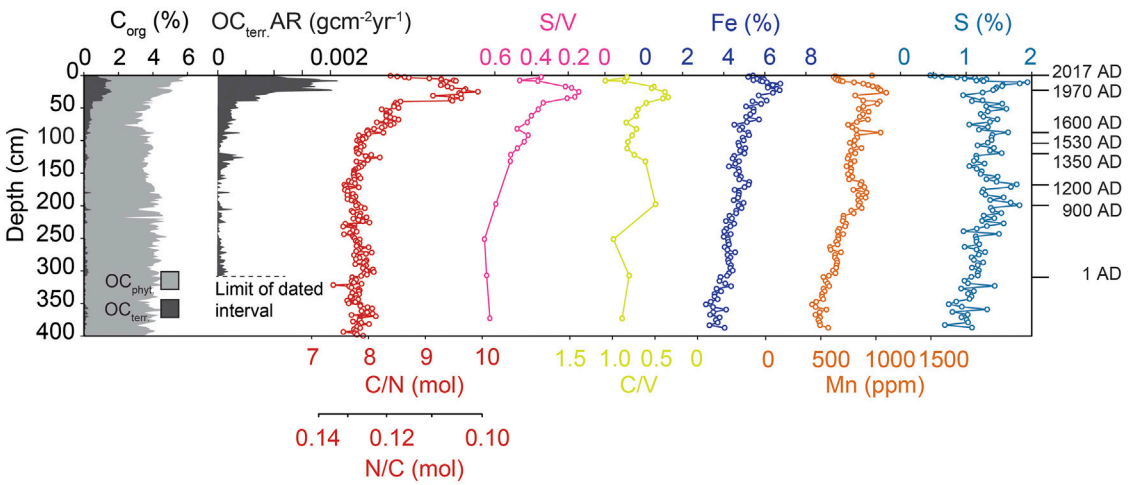

FIGURE 3 | Solid-phase components of the sediments at the Storfjärden site. The figure combines data from the GEMAX core of April 2015 (0–40 cm) and the piston core of September 2017 (40–400 cm). Fractions of C_{org} derived from phytoplankton ($OC_{phyt.}$) and terrestrial organic matter ($OC_{terr.}$) were calculated from N/C data using **Eq. 3** and **Eq. 4**. Dates on the right-hand margin correspond to tie-points in the Pb_{tot}-based age vs depth model (**Figure 2**).

RESULTS

Sedimentation Rate and Mass Accumulation Rate

The age vs depth model shows that the 4-m studied interval covers at least the last two millennia (**Figure 2**), with the earliest dating tie-point identified as 1 AD (as per Zillen et al., 2012). Both LSR and MAR have varied over the studied interval, showing ranges of 0.1–0.5 cm/yr and 0.04–0.15 g/cm^2/yr, respectively. The most recently deposited interval (1970–present) is characterized by relatively high values compared to the preceding 500 years (LSR = 0.49 cm/yr, MAR = 0.13 g/cm^2/yr), indicating enhanced inputs of sediment at this site in the recent past. One earlier interval of comparably high LSR and MAR values is observed deeper in the sediment column, corresponding to 1200–1350 AD.

Solid-Phase Profiles

Major changes occurred in bulk composition during the deposition of the uppermost meter of the sediments, corresponding to the interval since AD 1600 (**Figure 3**). Most importantly, this interval is characterized by an increase in organic matter content, as evidenced by elevated C_{org} values

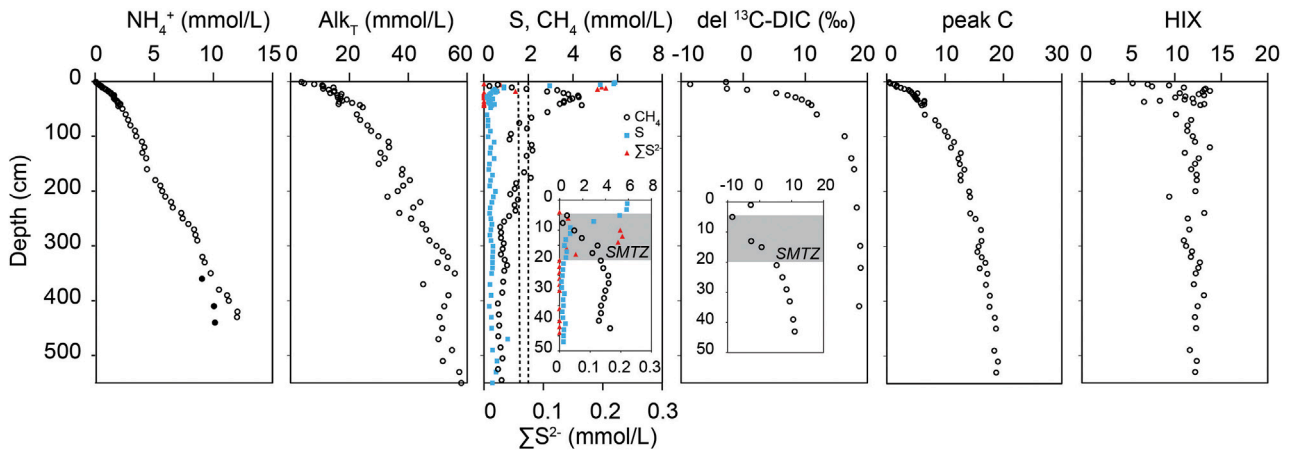

FIGURE 4 | Porewater profiles from the Storfjärden site. The figure combines data from multiple GEMAX and piston cores as described in **Table 1**. In all cases, the uppermost 40–60 cm derive from GEMAX cores preserving the sediment-water interface. Inserts show expanded profiles through the SMTZ. Note that sulfur (S) is considered to represent SO_4^{2-} (see text). Vertical dashed lines indicate saturation range of CH_4 at 1 atm pressure and 7.5–15ºC (bottom water temperature and air temperature on deck). Peak C = humic-like DOM fluorescence; HIX = DOM humification index.

up to 4–6% by weight (relative to <4% deeper in the sediments). Changes in the inputs of both terrestrial and phytoplankton-derived OM are responsible for this general increase, although the evolution of the two components since AD 1600 differs markedly (**Supplementary Figure S1**). While $OC_{phyt.}$ shows fairly stable contents until ~AD 1900 and a steady rise thereafter, $OC_{terr.}$ shows a steady rise from AD 1600 to ~AD 1850, followed by two abrupt increases between the mid-19th century and mid-20th century. Here we note that the absolute ages of events within the interval between the tie-points of AD 1600 and AD 1970 are subject to uncertainty as defined by the age vs depth model (**Figure 2**). In particular, it is plausible that sedimentation rate began to increase in parallel with changes in sediment composition, whereas the age model assumes linear sedimentation between the two tie-points. This would have the effect of making the estimated dates too old in the interval of most rapid compositional changes.

When the contributions of $OC_{phyt.}$ and $OC_{terr.}$ are combined, we observe that a significant fraction of total C_{org} in the late 20th century sediments (up to 30% according to **Eq. 3** and **Eq. 4**) is provided by terrestrial material (**Figure 3**). This fraction is far higher than in the deeper sediments, indicating a relative increase in $OC_{terr.}$ input over time. Furthermore, the absolute accumulation rate of $OM_{terr.}$ during this interval (up to 0.002 $gcm^{-2}yr^{-1}$) is unprecedented in the record (**Figure 3**). The accumulation rate of $OM_{terr.}$ has declined since the late 20th century maximum but the surface-sediment C/N ratio, and thus the calculated contribution of $OM_{terr.}$, remains elevated with respect to the deeper sediments.

Similar profiles to that of $OC_{terr.}$ are observed in the ratios of syringyl to vanillyl (S/V) and cinnamyl to vanillyl (C/V) phenols. Both the S/V and C/V phenol ratios show pronounced minima during the interval of maximum accumulation rate of $OM_{terr.}$ (**Figure 3**). However, the absolute ranges of S/V (0.1–0.6) and C/V (0.3–1.0) are similar to those observed in previous studies of lignin phenols in Baltic Sea sediments (Miltner and Emeis, 2001). Iron (Fe) and manganese (Mn) contents show a parallel evolution throughout the sediment record. Both elements' contents show a general increase from the core base upwards, towards maximum values of 6.7% (Fe) and 0.1% (Mn) within the interval of maximum $OM_{terr.}$ accumulation. Contents of Fe and Mn decline from this layer towards the sediment surface but the uppermost sample shows elevated values for both elements. Sulfur (S) displays a distinctly different profile, with higher variability throughout the record, and a pronounced maximum at 11 cm depth, clearly shallower than the maxima in $OM_{terr.}$, Fe and Mn.

Porewater Profiles

Porewater NH_4^+ and Alk_T show increasing concentrations with increasing depth in the sediment column, towards values of approximately 10 mmol/L and 50 mmol/L, respectively at 400 cm depth (**Figure 4**). The degree of curvature in both profiles is greatest in the uppermost 50 cm of the sediments, while the gradients below this depth are quite linear. Porewater CH_4 concentrations show a distinct maximum of >4 mmol/L at approximately 25 cm depth, very close to the 1970 horizon at the center of the layer of enhanced $OM_{terr.}$ deposition (**Figure 3**). A steep upwards gradient in CH_4 concentrations is observed between this layer and the SMTZ, defined as the interval of detectable porewater $\sum S^{2-}$ concentrations and encompassing the depth of equal concentrations of CH_4 and S (assumed equivalent to SO_4^{2-}). Below the porewater CH_4 maximum, a reverse gradient is observed towards background concentrations of ~1 mmol/L below 3 m depth. We cannot rule out that this gradient is an artefact of degassing effects due to the use of non-pressurized coring apparatus, and that true porewater CH_4 concentrations at depth are much higher as described in e.g. Egger et al. (2016). The increasing NH_4^+ and Alk_T concentrations below this horizon would support such a hypothesis, since all three species are

produced during methanogensis. However, it is also possible that the profile is genuine, and that the linear NH_4^+ and Alk_T gradients reflect upwards diffusion of these species from a deep source. We note that measured CH_4 concentrations decline to values well below the saturation concentration range during sampling on deck (1.6–2.0 mmol/L, **Figure 3**), whereas degassing typically leads to a plateau of values close to this range (Egger et al., 2016). This observation would support the hypothesis of a genuine reverse gradient in porewater CH_4. Above the SMTZ, concentrations of dissolved S (assumed equivalent to SO_4^{2-}) rise steeply towards the bottom water concentration of approximately 6 mmol/L.

Porewater δ^{13}C-DIC values show a minimum of −8.5‰ close to the SMTZ, while the uppermost measured sample at 1 cm depth has a value of −2.8‰. Below the SMTZ, δ^{13}C-DIC values show an asymptotic increase towards a stable value of +18–+19‰ in the deeper sediments. In terms of the CDOM optical properties of the porewaters, the peak C (considered to approximate the concentration of humic-like DOM; Coble, 1996) shows a generally concave profile similar to those of NH_4^+ and Alk_T. In contrast, the humification index (HIX; representing the extent of humification of the CDOM pool, Zsolnay et al., 1999) shows elevated values of up to 14 in the interval of enhanced $OM_{terr.}$ accumulation, superimposed on a trend from lower values at the surface (<6) to a consistent background of 10–12 at depth.

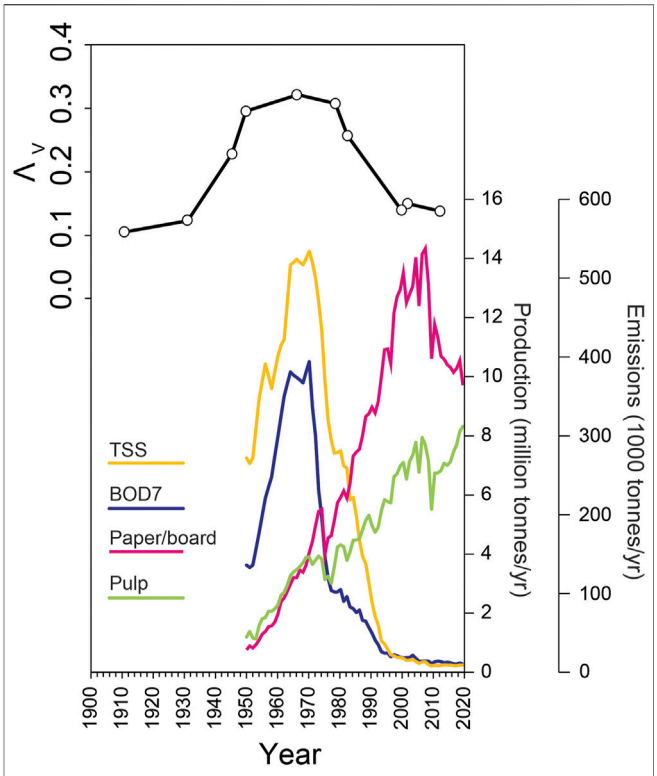

FIGURE 5 | Time series of production and emissions from forest industries in Finland since 1950 (https://www.forestindustries.fi/statistics/environment/), compared with the dated sediment record of total vanillyl phenols, reported as mg/100 g C (Λ_V). TSS = total suspended solids, BOD_7 = 7th day biological oxygen demand.

DISCUSSION

Terrestrial Organic Matter Loading to the Sediments During the 20th Century

Many coastal areas of the Baltic Sea show evidence for anthropogenic eutrophication (Conley et al., 2011) which often leads to enhanced carbon loading to sediments (Jokinen et al., 2018; Helmond et al., 2020). At Storfjärden, we observe a steady rise in OC_{phyt} contents in the period since ~AD 1900 (**Supplementary Figure S1**), consistent with eutrophication. However, a novel observation of this study is that a significant proportion of the additional recent carbon at this site is derived from terrestrial sources. The coincident minima in C/V and S/V phenol ratios during the period of maximum $OM_{terr.}$ accumulation rates indicate a shift towards more gymnosperm-dominated material (lower S/V phenol ratio) simultaneously with a shift towards more woody material (lower C/V phenol ratio, see **Table 2**), implying inputs of material originally derived from the Finnish forests.

Recent changes in C/V and S/V phenol ratios in estuarine settings have previously been interpreted as evidence for inputs of lignin-rich waste products from pulp and paper industries in North America (Louchouarn et al., 1999; Brandenberger et al., 2011). Such an interpretation appears plausible also for Storfjärden. Pulp production at Lohja, in the catchment of the River Mustionjoki (**Figure 1**), began in 1907 while paper production began in 1938 Heikkinen (2000). By 1957, the site was operating two paper machines with a combined potential output of 70 kt/y. Considering the uncertainty of the age vs depth model in this interval, the abrupt increases in $OC_{terr.}$ observed in **Supplementary Figure S1** could well relate to these major changes in industrial activity in the catchment. We also note that sedimentary contents of $OC_{terr.}$ were already increasing for several centuries prior to this time, indicating additional inputs potentially from land use change prior to the onset of industrial activity (e.g. Yang et al., 2021).

Emissions of waste products from forest industries are expected to be a function of the scale of operations, as well as the degree of waste water treatment, both of which may change over time (Katko et al., 2005). Data from the website of Finnish Forest Industries (https://www.forestindustries.fi/statistics/environment/) show that national estimates of total suspended solids (TSS) and 7th-day biological oxygen demand (BOD_7; a proxy for organic matter) emissions from forest industries to Finnish aquatic systems peaked in the period 1950–1980 (**Figure 5**). The decline in emissions since this period is primarily due to the introduction of on-site water recycling, sedimentation ponds and activated sludge treatment (Luonsi et al., 1988; Saunamäki, 1997; Katko et al., 2005). Such improvements were also enacted at the industrial sites in Lohja, reducing emissions significantly despite ongoing high levels of production until closure of operations in 2015.

A comparison of the time series of TSS and BOD_7 with the sedimentary content of vanillyl phenol oxidation products (Λ_V) at Storfjärden clearly shows the coincidence of maximum late

TABLE 3 | Estimate of carbon stored in fiber banks and fiber-rich sediments of 29 mapped locations in the Swedish coastal zone (Norrlin and Josefsson, 2017).

	Fiberbanks	Fiber-rich sediments	Total
Volume of wet sediment in 29 mapped locations, km^{3a}	0.007	0.011	
Volume of solid material, km^{3b}	0.0007	0.0011	
Mass of solid material (kilotonnes)[c]	1400	2750	
Mass of carbon (kilotonnes)[d]	210	129	339

[a]*Data provided in* ***Table 1*** *of Norrlin and Josefsson (2017).*
[b]*Estimated assuming volumetric porosity of 0.9 for both fiberbanks and fiber-rich sediments.*
[c]*Estimated assuming solid-phase density of 2.0 g* cm^{-3} *(fiberbanks) and 2.5 g* cm^{-3} *(fiber-rich sediments).*
[d]*Estimated from geometric mean* $\%C_{org}$ *of sediments from the Väja site (fiberbanks = 15%,* n = *4; fiber-rich sediments = 4.7%,* n = *4).*

20th century lignin accumulation with maximum emissions from forest industries in Finland (**Figure 5**, note that age vs depth uncertainties are lower in this interval due to the tie-point at 1970). Furthermore, Heikkinen (2000) reported high contents of sedimentary resin acids during the same period in the southern part of Lake Lohjanjärvi, adjacent to the industrial site (**Figure 1**), while high contents of $OM_{terr.}$ in sediments close to Storfjärden were reported by Jokinen et al. (2020). Combined, these studies strongly support the interpretation that emissions from industries in Lohja were the main reason for the high inputs of $OM_{terr.}$ to Storfjärden during the late 20th century. This observation is remarkable, as it implies that significant amounts of waterborne waste materials were transported through Lake Lohjanjärvi, the Mustionjoki river and Pojo Bay as far as the archipelago area where the study site is situated, a linear distance of over 60 km (**Figure 1**).

An ongoing mapping exercise in the Swedish coastal zone has identified 29 locations of fiberbank deposits close to point source industrial sites (Norrlin and Josefsson, 2017). In terms of surface area at any given location, true fiberbanks (sediments dominated by coarse waste material fibers) typically occupy up to 10 hectares, while fiber-rich sediments (sediments with visible fibers) may extend over up to 1 square kilometer. Our data raises the possibility that the true spatial extent of anthropogenic $OM_{terr.}$ inputs to sediments of the northern Baltic Sea may be larger, due to the transport of finer particulate and dissolved material away from point sources. Using the Swedish coastal area as an example due to the good data coverage, we performed a speculative mass balance calculation to investigate the scale of carbon accumulation in mapped fiberbank locations in relation to total inputs from forest industry sources (**Table 3**). From the reported sediment carbon concentrations in Dahlberg et al. (2020), we estimate that 0.34 million tonnes of carbon currently reside in the fiberbanks and fiber-rich sediments at the 29 mapped locations of Norrlin and Josefsson (2017). We subsequently derived a first-order estimate for the magnitude of forest industry carbon inputs to the Baltic Sea from Sweden. This estimate is based on an assumed Gaussian distribution of total COD emissions from Swedish forest industries over the period 1930–2000, fitted to the existing data from the Swedish Forest Industries Federation (**Supplementary Figure S2**) and corrected downwards assuming that only 5–15% of Swedish forest industry point source emissions enter the Baltic Sea, based on the locations of point sources in the maps of Norrlin and Josefsson (2017). The conversion from COD to total organic carbon (TOC) is based on the regression for high-latitude systems presented by Jiao et al. (2021). This exercise yields a total carbon input of 3.2–9.5 million tonnes, up to an order of magnitude greater than the estimated carbon stock in the 29 mapped locations (**Table 4**). Approximately half of the expected Swedish coastal point sources to the Baltic Sea have been mapped, thus its seems likely that the total fiberbank and fiber-rich sediment carbon stock in the Swedish coastal zone, once known, will be significantly less than the total input of carbon from anthropogenic $OM_{terr.}$ during 1930–2000. In this context, a diffuse contribution of anthropogenic $OM_{terr.}$ to a larger coastal sediment area is plausible, although part of the difference may be explained by mineralization and other transformations in the coastal environment.

Additionally, we estimated the quantitative significance of anthropogenic $OM_{terr.}$ inputs in the context of total terrestrial carbon loading to the Baltic Sea from Finland and Sweden. During the period 1993–2012, when standardized TOC analysis protocols were routinely used and therefore data are most reliable (Asmala et al., 2019), annual TOC loading to the Baltic Sea from the two countries combined varied from approximately 1.0–2.5 million tonnes per year (**Table 4**). Using the same Gaussian approach described above to provide a first-order estimate of the historical point source anthropogenic $OM_{terr.}$ inputs from Finland (**Supplementary Figure S2**) we calculate a total loading during the period 1930–2000 of approximately 4–13 million tonnes of TOC for the two countries combined. During the loading maximum of the mid-1960s, we estimate approximately 0.18–0.53 million tonnes TOC per year. In conclusion, during the period of maximum emissions, carbon inputs from industrial sources may have been a significant component (up to >10%) of total annual carbon loading from Finland and Sweden, although the contribution likely declined steeply during the last decades of the 20th century.

Overall Impact of Carbon Loading on Sediment Diagenesis

The additional carbon loading from both aquatic primary production and terrestrial sources has contributed to higher LSR and MAR at Storfjärden in the recent past, and driven high rates of remineralization in the upper sediments, as

TABLE 4 | Estimate of total carbon emissions to the Baltic Sea from forest industry point sources in Finland and Sweden during 1930–2000.

	Finland	Sweden	Total
Forest industry emissions 1930–2000			
Modeled integrated BOD[a] or COD[b] 1930–2000 (kilotonnes)	9496	69973	
Modeled integrated TOC[c] 1930–2000 (kilotonnes)	24350	63612	
Modeled integrated TOC to Baltic Sea 1930–2000 (kilotonnes, 5%)[d]	1217	3181	4398
Modeled integrated TOC to Baltic Sea 1930-2000 (kilotonnes, 15%)[e]	3652	9542	13194
Modeled max. annual TOC to Baltic Sea 1965 (kilotonnes, 5%)	49	127	176
Modeled max. annual TOC to Baltic Sea 1965 (kilotonnes, 15%)	146	380	527
Total riverine carbon inputs to Baltic Sea			
TOC to Baltic Sea 1993–2012 (kilotonnes/yr)[f,g]			
High	1148	1399	2547
Low	404	547	961

[a]*Total emissions in Finland, modeled using data for BOD_7 from Finnish Forest Industries from 1950 to 2000 (**Figure 5**) with hindcasting to 1930 assuming a Gaussian distribution (**Supplementary Figure S2**).*
[b]*Total emissions in Sweden, modeled using data for COD from Swedish Forest Industries Federation from 1978 to 2000 and hindcasted to 1930 assuming a parallel Gaussian distribution to that observed in Finland (**Supplementary Figure S2**).*
[c]*Estimated using the regressions for BOD and COD vs DOC in high-latitude systems presented in Jiao et al. (2021), assuming DOC = TOC.*
[d]*5% of modeled integrated TOC emissions 1930–2000.*
[e]*15% of modeled integrated TOC emissions 1930–2000.*
[f]*Data from Asmala et al. (2019)*
[g]*Data from Baltic Environmental Database.*

shown by the curvature of the NH_4^+ and Alk_T profiles in the upper 50 cm. The porewater data suggest that enhanced demand for electron acceptors has driven a rearrangement of the diagenetic zones in the upper sediment column (e.g., Middelburg and Levin, 2009). Most notably, carbon loading has enhanced methanogenesis and consequently shoaled both the interval of organoclastic sulfate reduction and the SMTZ. This sequence of eutrophication-driven changes in diagenetic zonation in the northern Baltic Sea has been described in several previous studies (e.g., Slomp et al., 2013; Egger et al., 2015; Rooze et al., 2016; Jilbert et al., 2018). A key piece of evidence for non-steady state conditions – the solid-phase S maximum indicating enhanced formation of sulfide minerals in the modern SMTZ – is observed in our profiles at 11 cm depth (**Figure 3**). Our data suggests that the methanogenic horizon is focused in the recently deposited sediments, with a gradient towards lower CH_4 concentrations observed in deeper layers. Even in the case of degassing impacting on the methane profile, the strong curvature of the NH_4^+ and Alk_T profiles in the upper 50 cm supports the theory that this interval is characterized by enhanced rates of methanogenesis relative to the rest of the sediment column. This confirms that enhanced methane production, and associated effluxes to the water column, are truly a legacy effect of recent carbon loading as postulated by Myllykangas et al. (2020a) from short-core data. Indeed, promotion of methanogenesis through rapid accumulation of organic material in sediments has been described previously in both freshwater and estuarine systems (e.g., Egger et al., 2016; Steinsberger et al., 2017). In the northern Baltic Sea, naturally low sulfate concentrations and modern high sedimentation rates allow degradable organic material to pass through the zone of sulfate reduction within the uppermost decimeters of the sediment column, thereby facilitating high rates of methanogenesis (e.g., Thang et al., 2013; Sawicka and Bruechert, 2017).

Methanogenesis, Organoclastic Sulfate Reduction and Anaerobic Oxidation of Methane

The shoaling of the diagenetic zones has triggered a cascade of secondary redox reactions in the sediment column at Storfjärden. Most importantly, the presence of methane in the shallow porewaters has likely led to the initiation of anaerobic oxidation of methane (AOM). Elevated rates of methane oxidation in the SMTZ at this site have been previously suggested from porewater data (Jilbert et al., 2018) and later confirmed by $^{14}CH_4$ incubations (Myllykangas et al., 2020b). The present study shows the enrichment of $\sum S^{2-}$ at the SMTZ reported in Jilbert et al. (2018) in the context of the wider porewater data (**Figure 4**). The enrichment is considered to indicate sulfide production via sulfate-mediated AOM (S-AOM):

$$CH_{4(aq)} + SO_{4(aq)}^{2-} + CO_{2(aq)} \rightarrow H_2S_{(aq)} + 2HCO_{3(aq)}^{-} + H_2O_{(l)} \quad (5)$$

To further investigate the dynamics of methanogenesis, organoclastic sulfate reduction and S-AOM at Storfjärden, we determined the δ^{13}C-DIC of porewaters throughout the core profile. Porewater δ^{13}C-DIC is influenced by each of these processes as described by Whiticar (1999) and Meister and Reyes (2019). Namely, organoclastic sulfate reduction depletes δ^{13}C-DIC from the bottom water value of ~0‰ towards the value of decaying organic matter (~−20‰). If S-AOM is active at the SMTZ, this process further depletes δ^{13}C-DIC due to consumption of isotopically light methane. In the underlying methanogenic zone, in contrast, δ^{13}C-DIC becomes enriched due to preferential consumption of

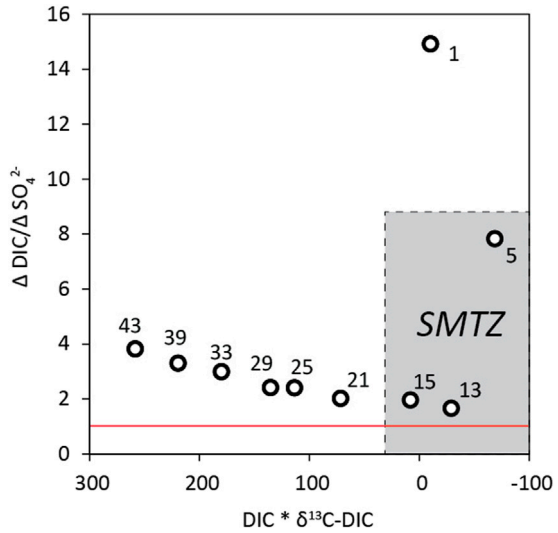

FIGURE 6 | Crossplot of $\Delta[DIC]/\Delta[SO_4^{2-}]$ vs. [DIC] * δ^{13}C-DIC for the upper sediment column, after Miller et al. (2017). Delta notation refers to change in concentration with respect to bottom water values. Numbers adjacent to data points indicate depth in cm. Horizontal red line shows the 1:1 ratio predicted for systems dominated by sulfate-mediated AOM (**Eq. 5**).

isotopically light DIC during hydrogenotrophic methanogenesis. The overall shape of the δ^{13}C-DIC profile at Storfjärden is consistent with those reported in other systems, with minimum values at or close to the SMTZ (e.g., Torres and Rugh, 2006; Chatterjee et al., 2011; Wehrmann et al., 2011; Yoshinaga et al., 2014). However we observe minimum δ^{13}C-DIC values of just −8.5‰ at 5 cm depth (**Figure 4**). Although low sampling resolution may have aliased the magnitude and precise depth of this minimum, the value is strongly enriched relative to those reported in the aforementioned studies. Below the SMTZ, δ^{13}C-DIC increases towards a stable background value of +18–+19‰. We interpret the generally enriched profile to indicate the presence of methanogenesis throughout the SMTZ (e.g., Thang et al., 2013) which dilutes the depletion of δ^{13}C-DIC expected from S-AOM and organoclastic sulfate reduction.

Previous studies have used variations on a crossplot of Δ[DIC] vs $\Delta[SO_4^{2-}]$ (the change in DIC and SO_4^{2-} concentrations relative to bottom water values) to attempt to quantify the relative importance of S-AOM and organoclastic sulfate reduction at the SMTZ (e.g., Kastner et al., 2008; Hu et al., 2015). The approach is based on the theory that AOM produces DIC and consumes SO_4^{2-} in a 1:1 ratio (**Eq. 5**) whereas for dissimilatory reduction the ratio is 2:1. Hence, the closer the value of $\Delta[DIC]/\Delta[SO_4^{2-}]$ is to 1, the greater the contribution of AOM. We chose to adopt the variation of Miller et al. (2017) to integrate δ^{13}C-DIC values into this analysis, in order to reduce the uncertainty introduced by unconstrained fluxes of DIC from deeper sediment layers (Chatterjee et al., 2011). Thus we plot $\Delta[DIC]/\Delta[SO_4^{2-}]$ against [DIC] * δ^{13}C-DIC (**Figure 6**, note that significant down-core changes in $[Ca^{2+}]$ are not observed in this system hence corrections to Δ[DIC] to account for carbonate mineral precipitation are neglected).

The relationship between $\Delta[DIC]/\Delta[SO_4^{2-}]$ and [DIC] * δ^{13}C-DIC strongly varies with depth in the upper sediment column (**Figure 6**). Samples from the SMTZ plot in the lower-right corner of the diagram, with $\Delta[DIC]/\Delta[SO_4^{2-}]$ values <2 coincident with negative [DIC] * δ^{13}C-DIC. Although the [DIC] * δ^{13}C-DIC values are less negative than observed in Miller et al. (2017) due to the diluting effect of methanogenesis in this system, the progression towards $\Delta[DIC]/\Delta[SO_4^{2-}]$ values <2 supports the hypothesis that sulfate-AOM occurs in the SMTZ. However, the minimum detected value for $\Delta[DIC]/\Delta[SO_4^{2-}]$ at 13 cm depth is 1.65, still significantly elevated with respect to the 1:1 value predicted from sulfate-AOM alone. This result suggests that an important fraction of total sulfate consumption is in the SMTZ is likely contributed by organoclastic sulfate reduction (e.g., Jorgensen et al., 2019). This is further supported by the relative diffusive fluxes of SO_4^{2-} and CH_4 into the SMTZ, which show a ratio of 2.66 (**Table 5**), clearly in excess of the 1:1 requirement of the reactants of sulfate-AOM (**Eq. 5**). Combined, the results imply that the SMTZ at our study site should be considered as a broad zone of overlapping diagenetic processes, in which methanogenesis, organoclastic sulfate reduction and S-AOM are all active simultaneously.

Consequences of the Shallow Sulfate-Methane Transition Zone at Storfjärden

The SMTZ at Storfjärden, similarly to much of the northern Baltic Sea today, is among the shallowest in the marine realm. Due to the strong correlation observed globally between SMTZ depth and associated diffusive fluxes of SO_4^{2-} and CH_4 (Egger et al., 2018), the values of these fluxes at Storfjärden are also high in global terms. Our calculated values for JCH_4 and JSO_4^{2-}, as well as the flux ratio of 2.66, fall within the ranges of compiled data for 40 marine coring sites with SMTZ depth <1 m (**Table 5**), suggesting that rates of methane-related processes at this site are typical for similar coastal locations of high carbon loading in the modern ocean.

While consumption of upwards-diffusing methane by AOM in marine sediments is considered near-quantitative on a global scale (Reeburgh, 2007; Saunois et al., 2016), sites with a shallow SMTZ often show inefficient AOM and significant fluxes of CH_4 to the water column and hence potentially to the atmosphere (e.g. Thang et al., 2013; Egger et al., 2016). Indeed, the Storfjärden area today is characterized by active fluxes of methane from sediments through both diffusion (Myllykangas et al., 2020a) and ebullition (Humborg et al., 2019). Our data confirms that the ultimate source of these emissions is the methanogenic layer in the late 20th century sediments, and hence that these emissions are a direct consequence of anthropogenic carbon loading through both eutrophication and inputs of OM_{terr}.

TABLE 5 | Comparison of fluxes of methane (JCH_4) and sulfate (JSO_4^{2-}) into the SMTZ at Storfjärden with 40 other locations in the marine realm with SMTZ depth < 1 m (data from Egger et al. (2018). Only sites with data for all parameters were used in the analysis.

	SMTZ depth (m)	JCH_4 (mmol/m^2/d)	JSO_4^{2-} (mmol/m^2/d)	JSO_4^{2-}:JCH_4
Storfjärden, Baltic Sea (this study)	0.12	1.73	4.59	2.66
40 sites of SMTZ < 1 m depth Egger et al. (2018)				
mean	0.44	1.81	1.31	1.38
min	0.04	0.07	0.06	0.60
max	1.00	15.93	13.07	3.69

Specific Impacts of $OM_{terr.}$ Inputs on Diagenetic Processes

Our data show indications that the additional loading of $OM_{terr.}$ during the 20th century has had specific impacts on diagenetic processes at Storfjärden. Terrestrial OM is traditionally considered to be relatively inert to remineralization in sediments (Hedges et al., 2000; Arndt et al., 2013) due to its refractory macromolecular composition (de Leeuw and Largeau, 1993) as well as protective associations formed with other materials prior to sedimentation (e.g., Hedges and Keil, 1995; Huguet et al., 2009). Indeed, lignin in sediments has been studied extensively as a biomarker for $OM_{terr.}$ largely due to its high preservation potential (Bianchi et al., 2018). However, several studies have reported that sites influenced by large direct inputs from forest industry display evidence for relatively high reactivity of this material in the sediment column. For example, high potential rates of methanogenesis were recently observed in wood fiber-rich sediments from the Finnish Lake Nasijärvi (Kokko et al., 2018). Similarly, fiber-rich sediments in Swedish coastal areas of the Baltic Sea support diffusive fluxes of organic contaminants to overlying waters, implying release from the solid-phase during diagenesis (Dahlberg et al., 2021).

At Storfjärden, we observe a maximum in the humification index (HIX) of porewater CDOM (values up to 14) coincident with the layer of enhanced $OM_{terr.}$ accumulation (**Figure 4**). This maximum is superimposed onto a trend from lower values at the surface (<6) to a consistent background of 10–12 at depth in the profile. Previous studies of HIX in sediment porewaters have typically interpreted this index as a proxy for CDOM sources in the degrading sedimentary OM, with low values (e.g. <3) indicative of autochthonous or microbial material and high values (e.g >6) indicative of terrestrial humic matter (Chen et al., 2016; Li et al., 2021). Our values are generally higher than those reported in these studies, implying an overall more humic composition of the source material. Furthermore, maximum values are observed in the layer of maximum $OM_{terr.}$ accumulation, suggesting solubilization of lignin and other terrestrial macromolecules, which are important components of humic-like CDOM (Del Vecchio & Blough, 2004). The underlying trend in HIX is also of interest. The observation of low-HIX CDOM in the shallowest layers and a stable background of high-HIX CDOM at depth implies a diagenetic shift in CDOM composition after sedimentation of degrading OM. Specifically, low-HIX CDOM produced during degradation in the shallowest layers appears to be consumed after release into the porewaters, leaving a residual accumulation of high-HIX CDOM at depth. We suggest that such consumption may occur through utilization of low-HIX DOM, which is considered more labile, by the microbial community. We note that the HIX profile contrasts with that of peak C, which shows a concave-down profile throughout the sediment column (**Figure 4**). This suggests that overall production of humic-like CDOM occurs similarly to that of inorganic degradation products such as NH_4^+ and Alk_T.

The additional flux of $OM_{terr.}$ to the coring location during the 20th century was likely accompanied by other terrestrial materials transported in association with organic matter. As described by Jokinen et al. (2020), metals such as Fe, Mn, Co, Cd, Pb, Sn and Zn are all enriched in the same depth interval as $OM_{terr.}$ in sediment cores from the Storfjärden area. Our long core data confirm that contents of Fe and Mn are higher in this layer than at any other depth in the sediment column (**Figure 3**). These metals derive from the terrestrial environment (including from anthropogenic sources), and are sedimented both as oxide minerals physically associated with organic matter, and as metal-OM complexes that undergo flocculation and aggregation at the estuarine salinity gradient (Widerlund and Ingri, 1996; Jilbert et al., 2018). Temporal changes in the inputs of oxides and metal-OM complexes may impact on diagenetic processes in several ways. For example, higher inputs of oxides may affect rates of oxide-mediated AOM (Lenstra et al., 2018) and thus the potential for phosphorus retention through vivianite formation (Slomp et al., 2013). Furthermore, complexation between OM and Fe in sediments has been shown to generally protect OM from remineralization and thus promote long-term carbon burial (Lalonde et al., 2012; Shields et al., 2016). Hence, not only the direct $OM_{terr.}$ inputs from forest industry themselves, but also the associated materials, may have altered diagenetic processes at Storfjärden during the 20th century.

CONCLUSION

This study shows that recent carbon loading to coastal sediments of the northern Baltic Sea has occurred not only as a consequence of increased aquatic primary production due to increased nutrient loading, but also of enhanced inputs of terrestrial organic matter from forest industry activities. This additional material has contributed to high sedimentation rates and demand for electron acceptors for organic matter remineralization, leading to a shoaling of the diagenetic zones in the sediment column. At the Storfjärden site, a distinct layer of elevated $OM_{terr.}$ contents in the late 20th century sediments are characterized by lignin phenol signatures typical of woody gymnosperm material, implying inputs from forest industries in the catchment. This layer coincides with high porewater methane concentrations and

high curvature in the profiles of NH_4^+ and Alk_T, indicating that the carbon loading has enhanced methanogenesis in the recently deposited sediments. Moreover, optical characteristics of porewater CDOM indicate active degradation of OM_{terr}. in the same layer. The SMTZ is observed directly above the methanogenic layer, and is characterized by sulfate-mediated AOM occurring alongside organoclastic sulfate reduction and methanogenesis. Fluxes of methane and sulfate into the SMTZ are high, but typical for similar eutrophic systems throughout the coastal oceans.

The broader spatial impact of anthropogenic OM_{terr}. inputs on coastal sediment biogeochemistry in the northern Baltic Sea remains to be established. Our data from Storfjärden shows that the signatures of such inputs may be identifiable several tens of kilometers from the industrial sources, confirming previous observations from the St. Lawrence estuary (Louchouarn et al., 1999). Moreover, our estimates of carbon storage in fiberbank locations in the Baltic Sea show that these proximal deposits are unlikely to account for the entire carbon loading from forest industry sources to the Baltic Sea during the 20th century. Determining the wider extent of anthropogenic OM_{terr}.-rich deposits in boreal coastal zones is essential for constraining carbon budgets in these areas, both in terms of carbon burial and greenhouse gas emissions.

DATA AVAILABILITY STATEMENT

All new data presented in the paper are accessible via Zenodo from 1 December 2021 (10.5281/zenodo.5570261) or directly from the corresponding author without undue reservation.

AUTHOR CONTRIBUTIONS

TJ devised the study, led the field and lab work and wrote the manuscript. GC and LL performed lignin phenol analyses and contributed to the interpretations and writing. SJ produced the age vs depth model and contributed to the interpretations and writing. EA performed the porewater CDOM analyses and contributed to the interpretations and writing. XS and CM performed the porewater $\delta^{13}C$ and Alkalinity analyses and contributed to the interpretations and writing. CH and AN co-ordinated the field campaigns with R/V Electra and contributed to the interpretations and writing.

FUNDING

This work was supported by Academy of Finland grants 317684 and 319956 and a University of Helsinki Tenure Track starting package to TJ. Support for a student exchange visit (LL) from Helsinki to Edinburgh was provided by University of Helsinki Department of Geosciences and Geography. The data in this study are contribution #5 from the Environmental and Mineralogical Laboratories (Hellabs) of the Department of Geosciences and Geography, University of Helsinki.

ACKNOWLEDGMENTS

This work forms part of the Baltic Bridge strategic partnership between the Stockholm University and the University of Helsinki. We thank the crew and captain of R/V Electra and technical staff at Tvärminne Zoological Station for support during field campaigns. We also thank all laboratory personnel who assisted with sample preparation and analytical work, especially Juhani Virkanen (University of Helsinki) and Steve Mowbray (University of Edinburgh).

SUPPLEMENTARY MATERIAL

The Supplementary Material for this article can be found online at: https://www.frontiersin.org/articles/10.3389/feart.2021.716416/full#supplementary-material

REFERENCES

Albert, D. B., Martens, C. S., and Alperin, M. J. (1998). Biogeochemical Processes Controlling Methane in Gassy Coastal Sediments-Part 2: Groundwater Flow Control of Acoustic Turbidity in Eckernförde Bay Sediments. *Continental Shelf Res.* 18, 1771–1793. doi:10.1016/S0278-4343(98)00057-0

Ali, M., and Sreekrishnan, T. R. (2001). Aquatic Toxicity from Pulp and Paper Mill Effluents: a Review. *Adv. Environ. Res.* 5, 175–196. doi:10.1016/S1093-0191(00)00055-1

Anderson, D. M., Glibert, P. M., and Burkholder, J. M. (2002). Harmful Algal Blooms and Eutrophication: Nutrient Sources, Composition, and Consequences. *Estuaries* 25, 704–726. doi:10.1007/BF02804901

Arndt, S., Jørgensen, B. B., LaRowe, D. E., Middelburg, J. J., Pancost, R. D., and Regnier, P. (2013). Quantifying the Degradation of Organic Matter in marine Sediments: A Review and Synthesis. *Earth-Science Rev.* 123, 53–86. doi:10.1016/j.earscirev.2013.02.008

Asmala, E., Bowers, D. G., Autio, R., Kaartokallio, H., and Thomas, D. N. (2014). Qualitative Changes of Riverine Dissolved Organic Matter at Low Salinities Due to Flocculation. *J. Geophys. Res. Biogeosci.* 119, 1919–1933. doi:10.1002/2014JG002722

Asmala, E., Carstensen, J., and Räike, A. (2019). Multiple Anthropogenic Drivers behind Upward Trends in Organic Carbon Concentrations in Boreal Rivers. *Environ. Res. Lett.* 14, 124018. doi:10.1088/1748-9326/ab4fa9

Asmala, E., Haraguchi, L., Markager, S., Massicotte, P., Riemann, B., Staehr, P. A., et al. (2018). Eutrophication Leads to Accumulation of Recalcitrant Autochthonous Organic Matter in Coastal Environment. *Glob. Biogeochem. Cycles* 32, 1673–1687. doi:10.1029/2017GB005848

Bange, H. W., Bartell, U. H., Rapsomanikis, S., and Andreae, M. O. (1994). Methane in the Baltic and North Seas and a Reassessment of the marine Emissions of Methane. *Glob. Biogeochem. Cycles* 8, 465–480. doi:10.1029/94GB02181

Beal, E. J., House, C. H., and Orphan, V. J. (2009). Manganese- and Iron-dependent marine Methane Oxidation. *Science* 325, 184–187. doi:10.1126/science.1169984

Berg, P., Risgaard-Petersen, N., and Rysgaard, S. (1998). Interpretation of Measured Concentration Profiles in Sediment Pore Water. *Limnol. Oceanogr.* 43, 1500–1510. doi:10.4319/lo.1998.43.7.1500

Bianchi, T. S., and Canuel, E. A. (2011). *Chemical Biomarkers in Aquatic Ecosystems*. Princeton, NJ: Princeton University Press.

Bianchi, T. S., Cui, X., Blair, N. E., Burdige, D. J., Eglinton, T. I., and Galy, V. (2018). Centers of Organic Carbon Burial and Oxidation at the Land-Ocean Interface. *Org. Geochem.* 115, 138–155. doi:10.1016/j.orggeochem.2017.09.008

Blair, N. E., and Aller, R. C. (2012). The Fate of Terrestrial Organic Carbon in the marine Environment. *Annu. Rev. Mar. Sci.* 4, 401–423. doi:10.1146/annurev-marine-120709-142717

Bonsdorff, E., Blomqvist, E. M., Mattila, J., and Norkko, A. (1997). Coastal Eutrophication: Causes, Consequences and Perspectives in the Archipelago Areas of the Northern Baltic Sea. *Estuarine, Coastal Shelf Sci.* 44, 63–72. doi:10.1016/S0272-7714(97)80008-X

Borges, A. V., and Abril, G. (2011). *Carbon Dioxide and Methane Dynamics in Estuaries*. San Diego; 525 B Street, Suite 1900 San Diego, CA 92101-4495 USA: Elsevier Academic Press Inc.

Boudreau, B. P. (1997). *Diagenetic Models and Their Implementation: Modelling Transport and Reactions in Aquatic Sediments*. Berlin-Heidelberg, Germany: Springer-Verlag.

Bowles, M. W., Mogollon, J. M., Kasten, S., Zabel, M., and Hinrichs, K.-U. (2014). Global Rates of marine Sulfate Reduction and Implications for Sub-sea-floor Metabolic Activities. *Science* 344, 889–891. doi:10.1126/science.1249213

Brandenberger, J. M., Louchouarn, P., and Crecelius, E. A. (2011). Natural and post-urbanization Signatures of Hypoxia in Two Basins of Puget Sound: Historical Reconstruction of Redox Sensitive Metals and Organic Matter Inputs. *Aquat. Geochem.* 17, 645–670. doi:10.1007/s10498-011-9129-0

Brännvall, M.-L., Bindler, R., Renberg, I., Emteryd, O., Bartnicki, J., and Billström, K. (1999). The Medieval Metal Industry Was the Cradle of Modern Large-Scale Atmospheric Lead Pollution in Northern Europe. *Environ. Sci. Technol.* 33, 4391–4395. doi:10.1021/es990279n

Breitburg, D., Levin, L. A., Oschlies, A., Grégoire, M., Chavez, F. P., Conley, D. J., et al. (2018). Declining Oxygen in the Global Ocean and Coastal Waters. *Science* 359, eaam7240. doi:10.1126/science.aam7240

Burton, E. D., Sullivan, L. A., Bush, R. T., Johnston, S. G., and Keene, A. F. (2008). A Simple and Inexpensive Chromium-Reducible Sulfur Method for Acid-Sulfate Soils. *Appl. Geochem.* 23, 2759–2766. doi:10.1016/j.apgeochem.2008.07.007

Canfield, D. E. (1991). Sulfate Reduction in Deep-Sea Sediments. *Am. J. Sci.* 291, 177–188. doi:10.2475/ajs.291.2.177

Carstensen, J., Conley, D. J., Bonsdorff, E., Gustafsson, B. G., Hietanen, S., Janas, U., et al. (2014). Hypoxia in the Baltic Sea: Biogeochemical Cycles, Benthic Fauna, and Management. *Ambio* 43, 26–36. doi:10.1007/s13280-013-0474-7

Chatterjee, S., Dickens, G. R., Bhatnagar, G., Chapman, W. G., Dugan, B., Snyder, G. T., et al. (2011). Pore Water Sulfate, Alkalinity, and Carbon Isotope Profiles in Shallow Sediment above marine Gas Hydrate Systems: A Numerical Modeling Perspective. *J. Geophys. Res.* 116, B09103. doi:10.1029/2011JB008290

Chen, M., Kim, J.-H., Nam, S.-I., Niessen, F., HongKang, W.-L. M.-H., Kang, M.-H., et al. (2016). Production of Fluorescent Dissolved Organic Matter in Arctic Ocean Sediments. *Sci. Rep.* 6, 39213. doi:10.1038/srep39213

Cline, J. (1969). Spectrophotometric Determination of Hydrogen Sulfide in Natural Waters. *Limnol. Oceanogr.* 14, 454–458. doi:10.4319/lo.1969.14.3.0454

Coble, P. G. (1996). Characterization of marine and Terrestrial DOM in Seawater Using Excitation-Emission Matrix Spectroscopy. *Mar. Chem.* 51, 325–346. doi:10.1016/0304-4203(95)00062-3

Conley, D. J., Björck, S., Bonsdorff, E., Carstensen, J., Destouni, G., Gustafsson, B. G., et al. (2009). Hypoxia-Related Processes in the Baltic Sea. *Environ. Sci. Technol.* 43, 3412–3420. doi:10.1021/es802762a

Conley, D. J., Carstensen, J., Aigars, J., Axe, P., Bonsdorff, E., Eremina, T., et al. (2011). Hypoxia Is Increasing in the Coastal Zone of the Baltic Sea. *Environ. Sci. Technol.* 45, 6777–6783. doi:10.1021/es201212r

Dahlberg, A.-K., Apler, A., Frogner-Kockum, P., Göransson, G., Snowball, I., Wiberg, K., et al. (2021). Dispersal of Persistent Organic Pollutants from Fiber-Contaminated Sediments: Biotic and Abiotic Pathways. *J. Soils Sediments* 21, 1852–1865. doi:10.1007/s11368-020-02871-1

Dahlberg, A.-K., Apler, A., Vogel, L., Wiberg, K., and Josefsson, S. (2020). Persistent Organic Pollutants in wood Fiber-Contaminated Sediments from the Baltic Sea. *J. Soils Sediments* 20, 2471–2483. doi:10.1007/s11368-020-02610-6

Dai, M., Yin, Z., Meng, F., Liu, Q., and Cai, W.-J. (2012). Spatial Distribution of Riverine DOC Inputs to the Ocean: an Updated Global Synthesis. *Curr. Opin. Environ. Sustainability* 4, 170–178. doi:10.1016/j.cosust.2012.03.003

de Leeuw, J. W., and Largeau, C. (1993). "A Review of Macromolecular Organic Compounds that Comprise Living Organisms and Their Role in Kerogen, Coal, and Petroleum Formation," in *Organic Geochemistry, Principles and Applications*. Editors M. H. Engel and S. A. Macko (New York: Plenum Press), 23–72. doi:10.1007/978-1-4615-2890-6_2

Dean, J. F., Middelburg, J. J., Röckmann, T., Aerts, R., Blauw, L. G., Egger, M., et al. (2018). Methane Feedbacks to the Global Climate System in a Warmer World. *Rev. Geophys.* 56, 207–250. doi:10.1002/2017RG000559

Deininger, A., and Frigstad, H. (2019). Reevaluating the Role of Organic Matter Sources for Coastal Eutrophication, Oligotrophication, and Ecosystem Health. *Front. Mar. Sci.* 6, 210. doi:10.3389/fmars.2019.00210

Del Vecchio, R., and Blough, N. V. (2004). On the Origin of the Optical Properties of Humic Substances. *Environ. Sci. Technol.* 38, 3885–3891. doi:10.1021/es049912h

Diaz, R. J., and Rosenberg, R. (2008). Spreading Dead Zones and Consequences for marine Ecosystems. *Science* 321, 926–929. doi:10.1126/science.1156401

Egger, M., Lenstra, W., Jong, D., Meysman, F. J. R., Sapart, C. J., van der Veen, C., et al. (2016). Rapid Sediment Accumulation Results in High Methane Effluxes from Coastal Sediments. *Plos One* 11, e0161609. doi:10.1371/journal.pone.0161609

Egger, M., Rasigraf, O., Sapart, C. J., Jilbert, T., Jetten, M. S. M., Röckmann, T., et al. (2015). Iron-mediated Anaerobic Oxidation of Methane in Brackish Coastal Sediments. *Environ. Sci. Technol.* 49, 277–283. doi:10.1021/es503663z

Egger, M., Riedinger, N., Mogollón, J. M., and Jørgensen, B. B. (2018). Global Diffusive Fluxes of Methane in marine Sediments. *Nat. Geosci* 11, 421–425. doi:10.1038/s41561-018-0122-8

Ettwig, K. F., Butler, M. K., Le Paslier, D., Pelletier, E., Mangenot, S., Kuypers, M. M. M., et al. (2010). Nitrite-driven Anaerobic Methane Oxidation by Oxygenic Bacteria. *Nature* 464, 543–548. doi:10.1038/nature08883

Gelesh, L. Marshall, K., Boicourt, W., and Lapham, L. (2016). Methane Concentrations Increase in Bottom Waters during Summertime Anoxia in the Highly Eutrophic Estuary, Chesapeake Bay, U.S.A. *Limnol. Oceanogr.* 61, S253–S266. doi:10.1002/lno.10272

Goñi, M. A., Teixeira, M. J., and Perkey, D. W. (2003). Sources and Distribution of Organic Matter in a River-Dominated Estuary (Winyah Bay, SC, USA). *Estuarine, Coastal Shelf Sci.* 57, 1023–1048. doi:10.1016/S0272-7714(03)00008-8

Gustafsson, B. G., Schenk, F., Blenckner, T., Eilola, K., Meier, H. E. M., Müller-Karulis, B., et al. (2012). Reconstructing the Development of Baltic Sea Eutrophication 1850-2006. *Ambio* 41, 534–548. doi:10.1007/s13280-012-0318-x

Hedges, J. I., and Ertel, J. R. (1982). Characterization of Lignin by Gas Capillary Chromatography of Cupric Oxide Oxidation Products. *Anal. Chem.* 54, 174–178. doi:10.1021/ac00239a007

Hedges, J. I., and Keil, R. G. (1995). Sedimentary Organic Matter Preservation: an Assessment and Speculative Synthesis. *Mar. Chem.* 49, 81–115. doi:10.1016/0304-4203(95)00008-F

Hedges, J. I., Mayorga, E., Tsamakis, E., McClain, M. E., Aufdenkampe, A., Quay, P., et al. (2000). Organic Matter in Bolivian Tributaries of the Amazon River: A Comparison to the Lower Mainstream. *Limnol. Oceanogr* 45, 1449–1466. doi:10.4319/lo.2000.45.7.1449

Heikkinen, P. (2000). *Paperitehtaan Jätevesikuormituksen Ympäristövaikutukset –sedimenttitutkimus Lohjanjärven Osuniemenlahdelta Ja Sen Lähiympäristöstä*. Turku: University of Turku, 1–143.

Heisler, J., Glibert, P. M., Burkholder, J. M., Anderson, D. M., Cochlan, W., Dennison, W. C., et al. (2008). Eutrophication and Harmful Algal Blooms: A Scientific Consensus. *Harmful Algae* 8, 3–13. doi:10.1016/j.hal.2008.08.006

Helmond, N. A. G. M., Lougheed, B. C., Vollebregt, A., Peterse, F., Fontorbe, G., Conley, D. J., et al. (2020). Recovery from Multi-millennial Natural Coastal Hypoxia in the Stockholm Archipelago, Baltic Sea, Terminated by Modern Human Activity. *Limnol. Oceanogr.* 65, 3085–3097. doi:10.1002/lno.11575

Holler, T., Wegener, G., Knittel, K., Boetius, A., Brunner, B., Kuypers, M. M. M., et al. (2009). Substantial13C/12C and D/H Fractionation during Anaerobic Oxidation of Methane by marine Consortia Enrichedin Vitro. *Environ. Microbiol. Rep.* 1, 370–376. doi:10.1111/j.1758-2229.2009.00074.x

Hu, Y., Feng, D., Liang, Q., Xia, Z., Chen, L., and Chen, D. (2015). Impact of Anaerobic Oxidation of Methane on the Geochemical Cycle of Redox-Sensitive Elements at Cold-Seep Sites of the Northern South China Sea. *Deep Sea Res. Part Topical Stud. Oceanography* 122, 84–94. doi:10.1016/j.dsr2.2015.06.012

Huguet, A., Vacher, L., Relexans, S., Saubusse, S., Froidefond, J. M., and Parlanti, E. (2009). Properties of Fluorescent Dissolved Organic Matter in the Gironde Estuary. *Org. Geochem.* 40, 706–719. doi:10.1016/j.orggeochem.2009.03.002

Humborg, C., Geibel, M. C., Sun, X., McCrackin, M., Mörth, C.-M., Stranne, C., et al. (2019). High Emissions of Carbon Dioxide and Methane from the Coastal Baltic Sea at the End of a Summer Heat Wave. *Front. Mar. Sci.* 6, 493. doi:10.3389/fmars.2019.00493

Jiao, N., Liu, J., Edwards, B., Lv, Z., Cai, R., Liu, Y., et al. (2021). Correcting a Major Error in Assessing Organic Carbon Pollution in Natural Waters. *Sci. Adv.* 7, eabc7318. doi:10.1126/sciadv.abc7318

Jilbert, T., Asmala, E., Schröder, C., Tiihonen, R., Myllykangas, J.-P., Virtasalo, J. J., et al. (2018). Impacts of Flocculation on the Distribution and Diagenesis of Iron in Boreal Estuarine Sediments. *Biogeosciences* 15, 1243–1271. doi:10.5194/bg-15-1243-2018

Jilbert, T., Jokinen, S., Saarinen, T., Mattus-Kumpunen, U., Simojoki, A., Saarni, S., et al. (2020). Impacts of a Deep Reactive Layer on Sedimentary Phosphorus Dynamics in a Boreal lake Recovering from Eutrophication. *Hydrobiologia* 847, 4401–4423. doi:10.1007/s10750-020-04289-9

Jilbert, T., and Slomp, C. P. (2013). Iron and Manganese Shuttles Control the Formation of Authigenic Phosphorus Minerals in the Euxinic Basins of the Baltic Sea. *Geochimica et Cosmochimica Acta* 107, 155–169. doi:10.1016/j.gca.2013.01.005

Jokinen, S. A., Jilbert, T., Tiihonen-Filppula, R., and Koho, K. (2020). Terrestrial Organic Matter Input Drives Sedimentary Trace Metal Sequestration in a Human-Impacted Boreal Estuary. *Sci. Total Environ.* 717, 137047. doi:10.1016/j.scitotenv.2020.137047

Jokinen, S. A., Virtasalo, J. J., Jilbert, T., Kaiser, J., Dellwig, O., Arz, H. W., et al. (2018). A 1500-year Multiproxy Record of Coastal Hypoxia from the Northern Baltic Sea Indicates Unprecedented Deoxygenation over the 20th century. *Biogeosciences* 15, 3975–4001. doi:10.5194/bg-15-3975-2018

Jørgensen, B. B., Beulig, F., Egger, M., Petro, C., Scholze, C., and Røy, H. (2019). Organoclastic Sulfate Reduction in the Sulfate-Methane Transition of marine Sediments. *Geochimica et Cosmochimica Acta* 254, 231–245. doi:10.1016/j.gca.2019.03.016

Jørgensen, B. B. (1982). Mineralization of Organic Matter in the Sea Bed-The Role of Sulphate Reduction. *Nature* 296, 643–645. doi:10.1038/296643a0

Kastner, M., Claypool, G., and Robertson, G. (2008). Geochemical Constraints on the Origin of the Pore Fluids and Gas Hydrate Distribution at Atwater Valley and Keathley Canyon, Northern Gulf of Mexico. *Mar. Pet. Geology.* 25, 860–872. doi:10.1016/j.marpetgeo.2008.01.022

Katko, T., Luonsi, A., and Juuti, P. (2005). Water Pollution Control and Strategies in Finnish Pulp and Paper Industries in the 20th century. *Ijep* 23, 368–387. doi:10.1504/IJEP.2005.007600

Knittel, K., and Boetius, A. (2009). Anaerobic Oxidation of Methane: Progress with an Unknown Process. *Annu. Rev. Microbiol.* 63, 311–334. doi:10.1146/annurev.micro.61.080706.093130

Kokko, M., Koskue, V., and Rintala, J. (2018). Anaerobic Digestion of 30–100-Year-Old Boreal lake Sedimented Fibre from the Pulp Industry: Extrapolating Methane Production Potential to a Practical Scale. *Water Res.* 133, 218–226. doi:10.1016/j.watres.2018.01.041

Koroleff, F. (1976). "Determination of Nutrients," in *Methods of Seawater Analysis*. Editors E. Grasshof, E. Kremling, and E. Weinhein (New York: Verlag Chemie).

Lacorte, S., Latorre, A., Barcelo, D., Rigol, A., Malmiqvist, A., and Welander, T. (2003). Organic Compounds in Paper-Mill Process Waters and Effluents. *Trac Trends Anal. Chem.* 22, 725–737. doi:10.1016/S0165-9936(03)01009-4

Lalonde, K., Mucci, A., Ouellet, A., and Gélinas, Y. (2012). Preservation of Organic Matter in Sediments Promoted by Iron. *Nature* 483, 198–200. doi:10.1038/nature10855

Lambert, T., Bouillon, S., Darchambeau, F., Morana, C., Roland, F. A. E., Descy, J.-P., et al. (2017). Effects of Human Land Use on the Terrestrial and Aquatic Sources of Fluvial Organic Matter in a Temperate River basin (The Meuse River, Belgium). *Biogeochemistry* 136, 191–211. doi:10.1007/s10533-017-0387-9

Landsman-Gerjoi, M., Perdrial, J. N., Lancellotti, B., Seybold, E., Schroth, A. W., Adair, C., et al. (2020). Measuring the Influence of Environmental Conditions on Dissolved Organic Matter Biodegradability and Optical Properties: a Combined Field and Laboratory Study. *Biogeochemistry* 149, 37–52. doi:10.1007/s10533-020-00664-9

Lenstra, W. K., Egger, M., van Helmond, N. A. G. M., Kritzberg, E., Conley, D. J., and Slomp, C. P. (2018). Large Variations in Iron Input to an Oligotrophic Baltic Sea Estuary: Impact on Sedimentary Phosphorus Burial. *Biogeosciences* 15, 6979–6996. doi:10.5194/bg-15-6979-2018

Leppäranta, M., and Myrberg, K. (2009). *Physical Oceanography of the Baltic Sea*. Heidelberg, Germany: Springer-Praxis.

Li, S., Lu, L., Wu, Y., Zhao, Z., Huang, C., Huang, T., et al. (2021). Investigation on Depth-dependent Properties and Benthic Effluxes of Dissolved Organic Matter (DOM) in Pore Water from Plateau lake Sediments. *Ecol. Indicators* 125, 107500. doi:10.1016/j.ecolind.2021.107500

Louchouarn, P., Lucotte, M., Canuel, R., Gagné, J.-P., and Richard, L.-F. (1997). Sources and Early Diagenesis of Lignin and Bulk Organic Matter in the Sediments of the Lower St. Lawrence Estuary and the Saguenay Fjord. *Mar. Chem.* 58, 3–26. doi:10.1016/S0304-4203(97)00022-4

Louchouarn, P., Lucotte, M., and Farella, N. (1999). Historical and Geographical Variations of Sources and Transport of Terrigenous Organic Matter Within a Large-Scale Coastal Environment. *Org. Geochem* 30, 675–699. doi:10.1016/S0146-6380(99)00019-4

Lougheed, B. C., and Obrochta, S. P. (2019). A Rapid, Deterministic Age-Depth Modeling Routine for Geological Sequences with Inherent Depth Uncertainty. *Paleoceanography and Paleoclimatology* 34, 122–133. doi:10.1029/2018PA003457

Luonsi, A., Junna, J., and Nevalainen, I. (1988). The Development of Waste Water Treatment in the Finnish Pulp and Paper Industry. *Water Sci. Technol.* 20, 25–36. doi:10.2166/wst.1988.0005

Martens, C. S., Albert, D. B., and Alperin, M. J. (1998). Biogeochemical Processes Controlling Methane in Gassy Coastal Sediments-Part 1. A Model Coupling Organic Matter Flux to Gas Production, Oxidation and Transport. *Continental Shelf Res.* 18, 1741–1770. doi:10.1016/S0278-4343(98)00056-9

Massicotte, P. (2019). eemR: Tools for Pre-processing Emission-Excitation Matrix (EEM) Fluorescence Data. R Package Version 1.0.1.

Massicotte, P., and Markager, S. (2016). Using a Gaussian Decomposition Approach to Model Absorption Spectra of Chromophoric Dissolved Organic Matter. *Mar. Chem.* 180, 24–32. doi:10.1016/j.marchem.2016.01.008

Mattsson, T., Kortelainen, P., and Räike, A. (2005). Export of DOM from Boreal Catchments: Impacts of Land Use Cover and Climate. *Biogeochemistry* 76, 373–394. doi:10.1007/s10533-005-6897-x

Mayer, L. M. (1994). Relationships between mineral Surfaces and Organic Carbon Concentrations in Soils and Sediments. *Chem. Geology.* 114, 347–363. doi:10.1016/0009-2541(94)90063-9

Meister, P., and Reyes, C. (2019). The Carbon-Isotope Record of the Sub-seafloor Biosphere. *Geosciences* 9, 507. doi:10.3390/geosciences9120507

Merkouriadi, I., and Leppäranta, M. (2015). Influence of Sea Ice on the Seasonal Variability of Hydrography and Heat Content in Tvärminne, Gulf of Finland. *Ann. Glaciol.* 56, 274–284. doi:10.3189/2015AoG69A003

Middelburg, J. J., and Levin, L. A. (2009). Coastal Hypoxia and Sediment Biogeochemistry. *Biogeosciences* 6, 1273–1293. doi:10.5194/bg-6-1273-2009

Miller, C. M., Dickens, G. R., Jakobsson, M., Johansson, C., Koshurnikov, A., O'Regan, M., et al. (2017). Pore Water Geochemistry along continental Slopes north of the East Siberian Sea: Inference of Low Methane Concentrations. *Biogeosciences* 14, 2929–2953. doi:10.5194/bg-14-2929-2017

Miltner, A., and Emeis, K. C. (2001). Terrestrial Organic Matter in Surface Sediments of the Baltic Sea, Northwest Europe, as Determined by CuO Oxidation. *Geochimica et Cosmochimica Acta* 65, 1285–1299. doi:10.1016/S0016-7037(00)00603-7

Mogollón, J. M., Dale, A. W., L'Heureux, I., and Regnier, P. (2011). Impact of Seasonal Temperature and Pressure Changes on Methane Gas Production, Dissolution, and Transport in Unfractured Sediments. *J. Geophys. Res.* 116, G03031. doi:10.1029/2010JG001592

Müller, C., Usbeck, R., and Miesner, F. (2016). Temperatures in Shallow marine Sediments: Influence of thermal Properties, Seasonal Forcing, and Man-Made Heat Sources. *Appl. Therm. Eng.* 108, 20–29. doi:10.1016/j.applthermaleng.2016.07.105

Myllykangas, J.-P., Hietanen, S., and Jilbert, T. (2020a). Legacy Effects of Eutrophication on Modern Methane Dynamics in a Boreal Estuary. *Estuaries and Coasts* 43, 189–206. doi:10.1007/s12237-019-00677-0

Myllykangas, J.-P., Rissanen, A. J., Hietanen, S., and Jilbert, T. (2020b). Influence of Electron Acceptor Availability and Microbial Community Structure on Sedimentary Methane Oxidation in a Boreal Estuary. *Biogeochemistry* 148, 291–309. doi:10.1007/s10533-020-00660-z

Nilsson, M. M., Hylén, A., Ekeroth, N., Kononets, M. Y., Viktorsson, L., Almroth-Rosell, E., et al. (2021). Particle Shuttling and Oxidation Capacity of Sedimentary Organic Carbon on the Baltic Sea System Scale. *Mar. Chem.* 232, 103963. doi:10.1016/j.marchem.2021.103963

Nixon, S. W. (1995). Coastal marine Eutrophication: A Definition, Social Causes, and Future Concerns. *Ophelia* 41, 199–219. doi:10.1080/00785236.1995.10422044

Norrlin, J., and Josefsson, S. (2017). Förorenade Fibersediment I Svenska Hav Och Sjöar. SGU Report 2017:07. Uppsala, Sweden: Geological Survey of Sweden. Available at: http://resource.sgu.se/produkter/sgurapp/s1707-rapport.pdf (Accessed October 14, 2021)

Pocklington, R., and Macgregor, C. D. (1973). The Determination of Lignin in Marine Sediments and Particulate Form in Seawater. *Int. J. Environ. Anal. Chem.* 3, 81–93. doi:10.1080/03067317308071070

Rabalais, N., Cai, W.-J., Carstensen, J., Conley, D., Fry, B., Hu, X., et al. (2014). Eutrophication-Driven Deoxygenation in the Coastal Ocean. *oceanog* 27, 172–183. doi:10.5670/oceanog.2014.21

Reeburgh, W. S. (2007). Oceanic Methane Biogeochemistry. *Chem. Rev.* 107, 486–513. doi:10.1021/cr050362v

Reed, D. C., Slomp, C. P., and Gustafsson, B. G. (2011). Sedimentary Phosphorus Dynamics and the Evolution of Bottom-Water Hypoxia: A Coupled Benthic-Pelagic Model of a Coastal System. *Limnol. Oceanogr.* 56, 1075–1092. doi:10.4319/lo.2011.56.3.1075

Reese, B. K., Finneran, D. W., Mills, H. J., Zhu, M.-X., and Morse, J. W. (2011). Examination and Refinement of the Determination of Aqueous Hydrogen Sulfide by the Methylene Blue Method. *Aquat. Geochem.* 17, 567–582. doi:10.1007/s10498-011-9128-1

Rooze, J., Egger, M., Tsandev, I., and Slomp, C. P. (2016). Iron-dependent Anaerobic Oxidation of Methane in Coastal Surface Sediments: Potential Controls and Impact. *Limnol. Oceanogr.* 61, S267–S282. doi:10.1002/lno.10275

Saunamäki, R. (1997). Activated Sludge Plants in Finland. *Sci. Technol.* 35, 235–243. doi:10.1016/S0273-1223(96)00936-510.2166/wst.1997.0527

Saunois, M., Bousquet, P., Poulter, B., Peregon, A., Ciais, P., Canadell, J. G., et al. (2016). The Global Methane Budget 2000-2012. *Earth Syst. Sci. Data* 8, 697–751. doi:10.5194/essd-8-697-2016

Sawicka, J. E., and Brüchert, V. (2017). Annual Variability and Regulation of Methane and Sulfate Fluxes in Baltic Sea Estuarine Sediments. *Biogeosciences* 14, 325–339. doi:10.5194/bg-14-325-2017

Schlünz, B., and Schneider, R. R. (2000). Transport of Terrestrial Organic Carbon to the Oceans by Rivers: Re-estimating Flux- and Burial Rates. *Int. J. Earth Sci.* 88, 599–606. doi:10.1007/s005310050290

Shields, M. R., Bianchi, T. S., Gélinas, Y., Allison, M. A., and Twilley, R. R. (2016). Enhanced Terrestrial Carbon Preservation Promoted by Reactive Iron in Deltaic Sediments. *Geophys. Res. Lett.* 43, 1149–1157. doi:10.1002/2015GL067388

Sholkovitz, E., Boyle, E., and Price, N. (1978). The Removal of Dissolved Humic Acids and Iron during Estuarine Mixing. *Earth Planet. Sci. Lett.* 40, 130–136. doi:10.1016/0012-821X(78)90082-1

Sivan, O., Adler, M., Pearson, A., Gelman, F., Bar-Or, I., John, S. G., et al. (2011). Geochemical Evidence for Iron-Mediated Anaerobic Oxidation of Methane. *Limnol. Oceanogr.* 56, 1536–1544. doi:10.4319/lo.2011.56.4.1536

Slomp, C. P., Mort, H. P., Jilbert, T., Reed, D. C., Gustafsson, B. G., and Wolthers, M. (2013). Coupled Dynamics of Iron and Phosphorus in Sediments of an Oligotrophic Coastal basin and the Impact of Anaerobic Oxidation of Methane. *Plos One* 8, e62386. doi:10.1371/journal.pone.0062386

Steinsberger, T., Schmid, M., Wüest, A., Schwefel, R., Wehrli, B., and Müller, B. (2017). Organic Carbon Mass Accumulation Rate Regulates the Flux of Reduced Substances from the Sediments of Deep Lakes. *Biogeosciences* 14, 3275–3285. doi:10.5194/bg-14-3275-2017

Thang, N. M., Brüchert, V., Formolo, M., Wegener, G., Ginters, L., Jørgensen, B. B., et al. (2013). The Impact of Sediment and Carbon Fluxes on the Biogeochemistry of Methane and Sulfur in Littoral Baltic Sea Sediments (Himmerfjärden, Sweden). *Estuaries and Coasts* 36, 98–115. doi:10.1007/s12237-012-9557-0

Tittel, J., Hüls, M., and Koschorreck, M. (2019). Terrestrial Vegetation Drives Methane Production in the Sediments of Two German Reservoirs. *Sci. Rep.* 9, 15944. doi:10.1038/s41598-019-52288-1

Torres, M. E., and Rugh, W. D. (2006). "Data Report: Isotopic Characterization of Dissolved Inorganic Carbon in Pore Waters Leg 204,". *Proc. ODP. Sci. Results. 204*. Editors A. M. Tréhu, G. Bohrmann, M. E. Torres, and F. S. Colwell. College Station,TX: Ocean Drilling Program, 1–16. doi:10.2973/odp.proc.sr.204.117.200

van der Veer, G. (2006). Geochemical Soil Survey of The Netherlands. Atlas of Major and Trace Elements in Topsoil and Parent Material; Assessment of Natural and Anthropogenic Enrichment Factors. *Neth. Geogr. Stud.* 347, 1–245. Available at: http://igitur-archive.library.uu.nl/dissertations/2006-1011-200742/full.pdf.

Virtasalo, J. J., Hämäläinen, J., and Kotilainen, A. T. (2014). Toward a Standard Stratigraphical Classification Practice for the Baltic Sea Sediments: the CUAL Approach. *Boreas* 43, 924–938. doi:10.1111/bor.12076

Virtasalo, J. J., Schröder, J. F., Luoma, S., Majaniemi, J., Mursu, J., and Scholten, J. (2019). Submarine Groundwater Discharge Site in the First Salpausselkä Ice-Marginal Formation, South Finland. *Solid Earth* 10, 405–423. doi:10.5194/se-10-405-2019

Weckström, K. (2006). Assessing Recent Eutrophication in Coastal Waters of the Gulf of Finland (Baltic Sea) Using Subfossil Diatoms. *J. Paleolimnol.* 35, 571–592. doi:10.1007/s10933-005-5264-1

Wehrmann, L. M., Risgaard-Petersen, N., Schrum, H. N., Walsh, E. A., Huh, Y., Ikehara, M., et al. (2011). Coupled Organic and Inorganic Carbon Cycling in the Deep Subseafloor Sediment of the Northeastern Bering Sea Slope (IODP Exp. 323). *Chem. Geology.* 284 (3-4), 251–261. doi:10.1016/j.chemgeo.2011.03.002

Whiticar, M. J. (1999). Carbon and Hydrogen Isotope Systematics of Bacterial Formation and Oxidation of Methane. *Chem. Geology.* 161, 291–314. doi:10.1016/S0009-2541(99)00092-3

Widerlund, A., and Ingri, J. (1996). Redox Cycling of Iron and Manganese in Sediments of the Kalix River Estuary, Northern Sweden. *Aquat. Geochem.* 2, 185–201. doi:10.1007/BF00121631

Yang, B., Ljung, K., Nielsen, A. B., Fahlgren, E., and Hammarlund, D. (2021). Impacts of Long-Term Land Use on Terrestrial Organic Matter Input to Lakes Based on Lignin Phenols in Sediment Records from a Swedish forest lake. *Sci. Total Environ.* 774, 145517. doi:10.1016/j.scitotenv.2021.145517

Yoshinaga, M. Y., Holler, T., Goldhammer, T., Wegener, G., Pohlman, J. W., Brunner, B., et al. (2014). Carbon Isotope Equilibration during Sulphate-Limited Anaerobic Oxidation of Methane. *Nat. Geosci* 7, 190–194. doi:10.1038/NGEO2069

Zillén, L., Lenz, C., and Jilbert, T. (2012). Stable lead (Pb) Isotopes and Concentrations - A Useful Independent Dating Tool for Baltic Sea Sediments. *Quat. Geochronol.* 8, 41–45. doi:10.1016/j.quageo.2011.11.001

Zsolnay, A., Baigar, E., Jimenez, M., Steinweg, B., and Saccomandi, F. (1999). Differentiating with Fluorescence Spectroscopy the Sources of Dissolved Organic Matter in Soils Subjected to Drying. *Chemosphere* 38, 45–50. doi:10.1016/S0045-6535(98)00166-0

Conflict of Interest: The authors declare that the research was conducted in the absence of any commercial or financial relationships that could be construed as a potential conflict of interest.

Publisher's Note: All claims expressed in this article are solely those of the authors and do not necessarily represent those of their affiliated organizations, or those of the publisher, the editors and the reviewers. Any product that may be evaluated in this article, or claim that may be made by its manufacturer, is not guaranteed or endorsed by the publisher.